Nano Today 57 (2024) 102337

Contents lists available at ScienceDirect

Nano Today

journal homepage: www.elsevier.com/locate/nanotoday

Review

Stimuli-triggered pollen-inspired micro/nanorobots for advanced therapeutics

Youjin Seol [a,b,1], Keya Ganguly [a,c,1], Hojin Kim [a,b], Aayushi Randhawa [a,b], Tejal V. Patil [a,b], Sayan Deb Dutta [a], Rumi Acharya [a,b], Ki-Taek Lim [a,b,c,*]

[a] Department of Biosystems Engineering, Kangwon University, Chuncheon, Gangwon-do 24341, Republic of Korea
[b] Interdisciplinary Program in Smart Agriculture, Kangwon National University, Chuncheon, Gangwon-do 24341, Republic of Korea
[c] Institute of Forest Science, Kangwon National University, Chuncheon, Gangwon-do 24341, Republic of Korea

ARTICLE INFO

Keywords:
Stimuli-responsive
Micro/nanorobot
Pollen-inspired
Adhesion
Advanced therapeutics

ABSTRACT

Stimuli-responsive micro/nanorobots have revolutionized biomedical research by overcoming the therapeutic limitations that require critical medical interventions. These micro/nanorobots are designed to move through the body's circulatory system and hold promise for advanced micro/nano surgery, targeted drug delivery, immunotherapy, and combating bacterial infections. The efficacy of these bots largely relies on specific physicochemical attributes (such as high biocompatibility, in vivo site-specific adhesion properties, high surface area at the nanoscale, ability to combat immune rejection and controlled actuation). Biomimetic pollen-like micro/nanorobots (P-M/N-bots), inspired by pollen, have emerged as suitable structures for *in vivo* applications. These structures are meticulously fabricated through the chemical modification of materials such as silica and zinc oxide. After fabrication, the micro/nanorobots' movement can be precisely controlled by different stimuli (such as near-infrared radiation (NIR), magnetic fields, and temperature variations, among others). Despite the growing scientific outcomes, we are yet to conduct a concise review of the development and progress of on-the-rise P-M/N-bots. Therefore, it is necessary to provide an overview of the current developments in intelligent P-M/N-bots to encourage future developments in this field. Hence, in this review, we discuss the synthesis methods for P-M/N-bots and feasible actuation methods, including NIR, magnetic field, pH, and temperature. We emphasize the various therapeutic applications of the P-M/N-bots in biomedical applications, focusing on anti-cancer therapies, targeted drug delivery, anti-bacterial effects, and curing inflammatory conditions. Furthermore, we discuss potential challenges in the clinical application of P-M/N-bots. Anticipating the future of this field, we believe that this review will serve as a valuable guide for the development of promising P-M/N-bots with enhanced therapeutic outcomes.

Introduction

Conventional medications and surgery often fail to manage critical cardiovascular diseases [1], cancer progression [2], severe infections [3], tissue regeneration [4], and precise drug administration [5]. In particular, drug accumulation at non-specific locations leads to systemic side effects and tissue damage [6]. Hence, a crucial objective of modern medicine is to devise precise therapies by developing innovative strategies, such as the utilization of micro/nanorobots (hereafter referred to as M/N-bots). M/N bots are capable of systemic circulation throughout the human body and can be controlled externally [7]. These M/N-bots have the potential for targeted invasive surgery, drug delivery, and disease treatment in hard-to-reach deep areas of the body, [8–15] lowering non-target toxicity and overcoming the limitations of existing treatments [16].

Over the past decade, studies have shown that the function of M/N-bots within the delicate physiological environment of the human body remains limited, resulting in undesired functionalities, such as low site-specific adhesion, low payload adhesion, insignificant tissue penetration, immune rejection, and challenging actuation mechanisms [17]. Therefore, M/N-bots with improved functionalities and stimuli-responsiveness are being engineered to address these difficulties,

* Corresponding author at: Department of Biosystems Engineering, Kangwon University, Chuncheon, Gangwon-do 24341, Republic of Korea.
E-mail address: ktlim@kangwon.ac.kr (K.-T. Lim).
[1] These authors have contributed equally to this manuscript.

https://doi.org/10.1016/j.nantod.2024.102337
Received 27 February 2024; Received in revised form 21 May 2024; Accepted 30 May 2024
Available online 3 June 2024

often by biomimicking nature-inspired structures. There are numerous examples of micro/nanostructures in plants and animals [18] and in their products, including the structural diversity observed in plant-derived pollen particles [19]. Pollen is a powdery material that is generated by the male reproductive organs of seed-bearing plants. These are vehicles for the transmission of male genetic material. The structure may be described as a hollow capsule that safeguards the enclosed genetic components along with other internal cellular organelles, shielding them from environmental damage. Additionally, it ensures secure adhesion to the floral stigma, facilitating pollination [20].

Pollen particles are typically small, in the nanometer range, and possess hollow structures.

[21–23]. The surface shape of the particles is crucial for controlling their interactions with cells, such as promoting strong adherence, enhancing cargo delivery, and improving tissue penetration, making pollen particles a key nanomaterial in M/N-bot fabrication. However, additional engineering efforts are required to address challenges related to immune rejection and desired actuation mechanisms [24] [25,26].

Several polymers were used to fabricate pollen-like M/N-bots (P-M/N-bots). For example, P-M/N-bots can be fabricated using materials, such as ZnO [27], gold (Au) [28], silicon [29], polydopamine [30], and poly (N-isopropylacrylamide) (pNIPAM) [31]. Furthermore, because precise motion control is crucial for P-M/N-bots to execute practical functions, stimuli-responsive biopolymers are incorporated to modify their surfaces for remote-control access [32–34]. To date, numerous stimuli (such as magnetic fields, temperature, light, and pH) have been reported to drive P-M/N-bots *in vitro* and *in vivo* [35–37]. By manipulating the stimuli-responsive parameters, it is possible to modify the speed, trajectory, and other aspects of P-M/N-bots [38].

To date, several stimuli-responsive M/N bots have been reviewed to date [39–42]. However, only a few reviews have been published on P-M/N-bots highlighting their promising progress in biomedical applications. Hence, this review provides an overview of the advancements in P-M/N-bot fabrication, stimuli-mediated actuation, and mode of action. First, we discuss the importance of pollen particles as desirable nanostructures in biomedicine, focusing on their diverse morphologies and unique microstructural architectures. We further elaborate on chemically synthesized artificial pollen-like nanostructures to concisely

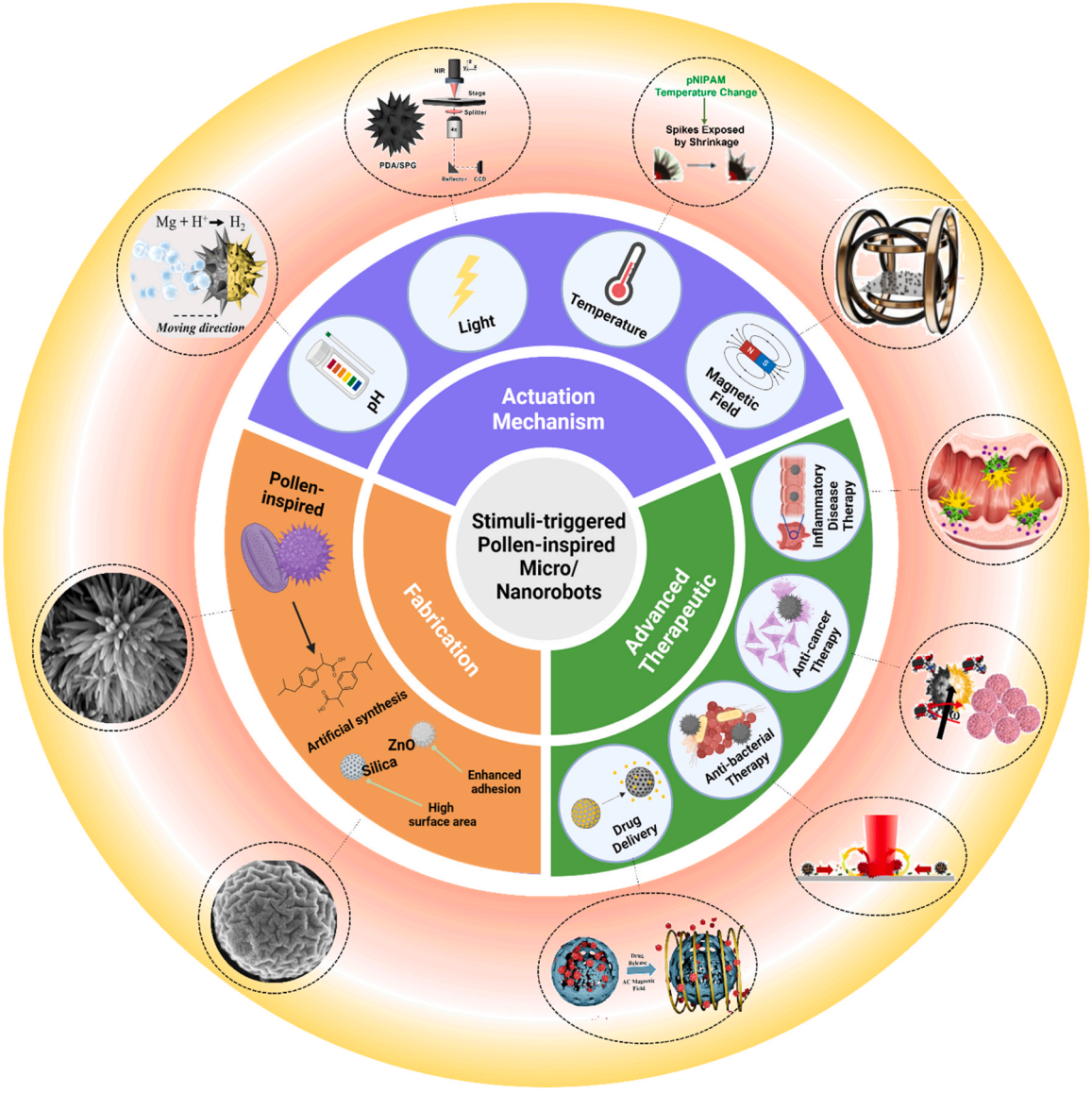

Fig. 1. Schematic overview of stimuli-triggered P-M/N bots for improved therapeutic; including fabrication of pollen-inspired ZnO (spiky) [27], pollen-inspired silica (mesoporous) [43], actuation mechanisms through pH [44], light [45], temperature [46], magnetic field [47], and therapeutic applications like inflammatory disease therapy [37], anti-cancer therapy [48], anti-bacterial therapy [45], and drug delivery [49].

review the fabrication processes used over the decades to produce pollen-like microparticles. Finally, we review P-M/N-bots in detail, specifically focusing on the actuation mechanism in bots that have transitioned from pollen-like particles into bots. We hope that through an exhaustive discussion of the natural pollen structure of the synthetic pollen-like micro/nanoparticles to the emergence of P-M/N-bots, we can obtain an overall picture of the development of these impressive microbots in biomedicine. We also explore the biocompatibility and biodegradation of P-M/N-bots within biological systems as well as the biological obstacles and constraints of current *in vivo* monitoring methods, suggesting directions for future research in this field. We anticipate that this review will aid in understanding the current state of the art of P-M/N-bots and encourage the development of advanced P-M/N-bots in the future (Fig. 1).

P-M/N structures

As mentioned earlier, pollen particles are the male reproductive units of fruit-bearing plants. Pollen from the same species is often uniform in shape and size, whereas pollen dimensions vary across species. Fig. 2A shows a few examples of variation in pollen shape and size across plant species [50]. These particles may have perfectly spherical shapes or edges that can take other forms. Additionally, they have smooth surfaces or surfaces with varied textures, such as spikes, grooves, or porous pits [51]. Despite their origin, the microstructures of most pollen particles exhibit a double-layer wall architecture. The inner layer, known as the intine, is composed of carbohydrates, such as cellulose and pectin, whereas the outer layer, known as the exine, is composed of sporopollenin, a chemically robust polymer [52,53]. Exines are extremely resistant to prolonged drying and various chemical attacks, making them one of the toughest and most durable materials[54]. The exine surface is coated with Pollenkitt, a sticky liquid that modulates the adhesive characteristics of pollen via a wetting mechanism [55].

For instance, adhesion tests with five distinct pollen species showed that the pollen with the highest adhesion was from the dandelion and sunflower, owing to the presence of the highest amount of Pollenkit on their echinate (spiky) surface, leading to high surface adhesion ability [25]. This is also due to the fact that pollens featuring spiky nanostructures have a larger surface area than other counterparts, such as the spherical pollens [25,56] [57,58]. This extensive surface area is beneficial for using pollen surfaces as nanocarriers for drug delivery and targeted adhesion to specific cells or organs. Similarly, the porous architecture, as observed in rape pollen, enhances the cargo-carrying capacity through its sizable internal pores and the creation of an extensive contact area. This attribute has versatile applications in the drug delivery and energy storage fields [59].

However, most pollens contain allergens, limiting their application. Consequently, the pollenkitt, intine, must be removed to achieve an empty sporopollenin shell [60–62]. Sporopolynerine-exine shells can be extracted using chemical, enzymatic, and combination techniques (Fig. 2B). When pollen is chemically treated, allergic ingredients are removed and the normally closed aperture is opened, resulting in a hole in the pollen wall (Fig. 2C, D) [63]. Drugs could be loaded and released through these apertures. Thus, pollen demonstrates an elevated capacity as micro/nano carriers.

Pollen-inspired micro and nano-structures have been artificially engineered using metals and polymers. In the next section, we describe the artificial synthesis of pollen-inspired micro/nano-structures, which have shown promising results in the development of nanocarriers with preferred physiochemical properties.

Artificially synthesized P-M/N structures without actuation

A global endeavor has been made to create micro/nanostructures that imitate the captivating surface characteristics of pollen. These P-M/N structures, which are devoid of actuation, are widely acknowledged for their improved bio-adhesion, surface penetration, effectiveness as drug carriers, and immune rejection. The most common method for producing P-M/N structures is chemical synthesis. Early P-M/N structures are mainly produced using metallic materials, primarily because of the simple synthesis methods linked to metals [66–69]. Through these synthesis techniques, the size, morphology, and surface characteristics of the P-M/N structures can be manipulated.

Metal/ metallic oxide-based P-M/N structures

The surface plasmon resonance properties, absorption capacity, and light scattering of metal nanoparticles are advantageous compared to those of other polymeric nanostructures. Therefore, they have been used extensively in bioimaging applications. Furthermore, nanosized metals have large surface areas that can be chemically and physically modified [70,71]. We also discuss the use of Au-, zinc oxide-, and silica based P-M/N structures for biomedical applications.

Nanometer-scale Au particles have been actively studied for a long time due to their optical properties. The manipulation of the nanoscale surface characteristics of Au nanoparticles (AuNPs) leads to adjustable optical properties. Spiky AuNPs exhibit enhanced surface plasmon resonance[72], augmented photothermal properties[73], and superior Raman scattering performance[74], which are attributable to their large surface areas. The production of spiked AuNPs can be divided into two main methods: (1) direct synthesis and (2) seed-mediated growth. Direct synthesis can create spiked nanoparticles by selecting the appropriate metal precursors and reducing agents and surfactants[75]. In contrast, seed-mediated growth methods utilize tiny metal seed nanoparticles, generally smaller than 10 nm, as nucleation points, and require the incremental addition of metal precursors and capping agents to foster the anisotropic development of spikes [76,77].

Au has been used to create biomimetic pollen structures in several ways. Kim et al., have reported the fabrication of a biomimetic nano-pine-pollen nanostructure-based surface-enhance Raman scattering (SERS) sensor for the detection of toxicants, such as heavy metal ions and amyloid-β oligomers. To fabricate the pine pollen structure, we fabricated an Au layer on a pollen-mimicking silver structure via a galvanic replacement reaction. The resulting Au layer enhanced the SERS response [78].

Zinc oxide is a substance with strong anti-bacterial properties that has uses ranging from electronics to sensors, photocatalysis, energy, and biomedicine[79–82]. Spherical ZnO oxide nanoparticles, the most representative form, have attracted interest because they are easily absorbed and metabolized by cells. Furthermore, it is toxic to tumor cells but not normal cells and exhibits a wide range of toxicity in a number of tumor cell lines[83–85]. Dang et al. compared the cytotoxic effects of spherical zinc oxide nanoparticles (SNPs) and spiked zinc oxide nanoparticles (SPNPs)[86]. Spiked zinc oxide particles were synthesized by the sequential self-assembly of zincate into nanoparticles, nanorods, nanoleaves, and finally, nanospikes, during the gradual conversion of Zn $(OH)_4^{2-}$ into hydroxyl ions (Fig. 3A-B). Zinc oxide nanoparticle-induced abnormalities in reactive oxygen species (ROS) and mitochondrial membrane potential (MMP) can lead to cell death. ROS generation (Fig. 3C) and loss of MMP (Fig. 3D) were observed when A549 (a human lung adenocarcinoma cell line) cells were treated with SPNPs and SNPs to generate nanostructures. A large amount of SPNP was found outside the plasma membrane of SPNP-treated A549 cells (Fig. 3E-E-i). These results showed that SPNP causes tumor cell death differently from SNP, which promotes cell death through intracellular entry.

Additionally, SPNP exhibited long-term and sustainable cytotoxic effects on A549 cells compared to SNP. Even when the recycling frequency was three cycles, the SPNPs exhibited an obvious cytotoxic effect (Fig. 3**F**). Even in the cell morphology observed after two cycles, the SPNPs remained (Fig. 3**G**). In 3D tumor cell spheroids, SPNP showed better cytotoxicity than SNP, with SNP treatment showing a decrease in the PI signal at a depth of nearly 50μm, while SPNP treatment showed a

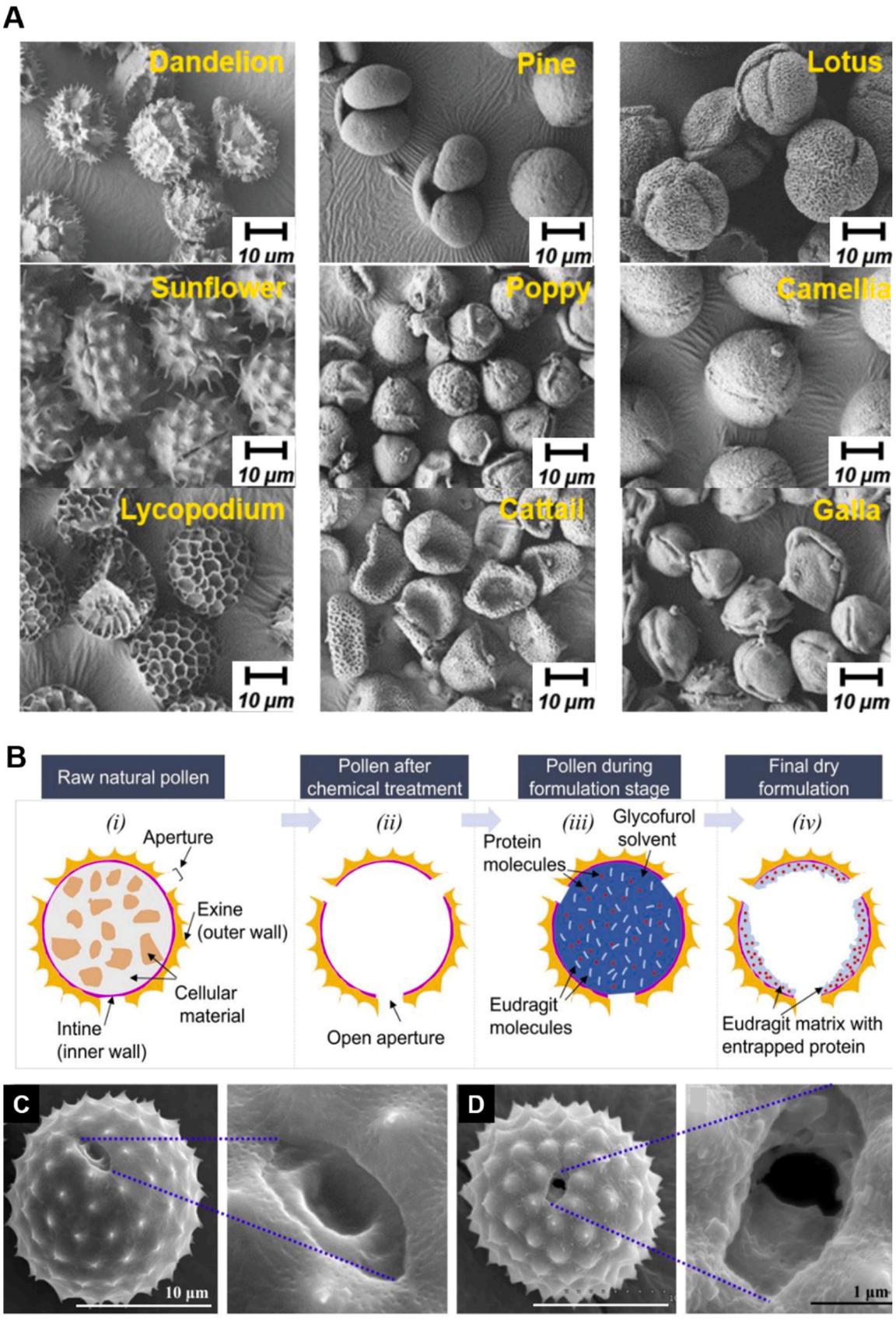

Fig. 2. (A) SEM images of nine different types of pollen [64]. (B) Schematic representation of the chemical treatment process to remove substances inside pollen. (C) Raw pollen with a closed aperture hole. (D) Processed pollen with an open aperture hole[65].

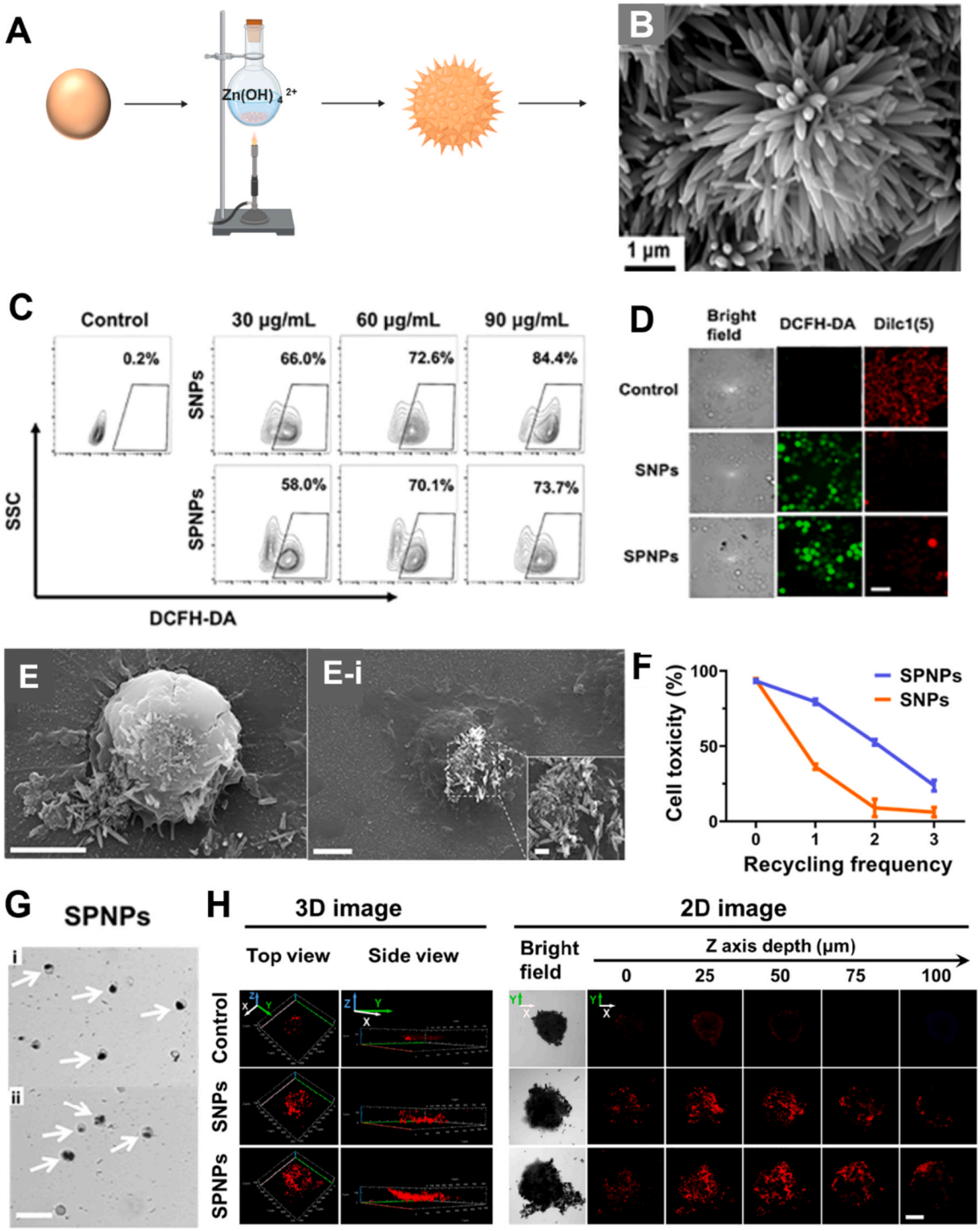

Fig. 3. (A) Schematic diagram of ZnO spiky nanoparticles (SPNPs) synthesis. (B) SEM image of SPNPs. (C) Flow cytometry-based quantitative measurement of ROS production using DCFH-DA staining. (D) Microscopic imaging of ROS production using DCFH-DA staining and Dilc1. (E, E-i) SEM characterization of A549 cells after incubation with ZnO SPNPs. (F) Statistical analysis of cytotoxicity counting cells remaining after recycling treatment. (G) Opaque structure of SPNPs covered on cells collected after 2 cycles. (H) Cytotoxicity of ZnO SNPs and SPNPs on 3D tumor cells spheroids[27].

maximum depth of 75μm (Fig. 3**H**).

Non-metal based P-M/N structures

Silica

Mesoporous silica nanoparticles (MSNs) were first known in the early 1990s using surfactants as structure-directing agents [87,88]. Mesoporous silica particles can be customized in terms of size,[89] shape,[90,91], and surface structure [92,93], and the synthesis method can be completely customized. Several recent reviews have examined various approaches for MSN synthesis [94–96]. Marjani et al. synthesized mesoporous silica particles resembling pollen (MI-PLMS) using a soft template hydrothermal approach[43]. The synthesized MI-PLMS exhibits a wrinkled exterior (Fig. 4A) and a multi-layered hollow structure (Fig. 4B), characteristic of pollen morphology. MI-PLMS has been employed as an adsorbent owing to its comparatively elevated surface

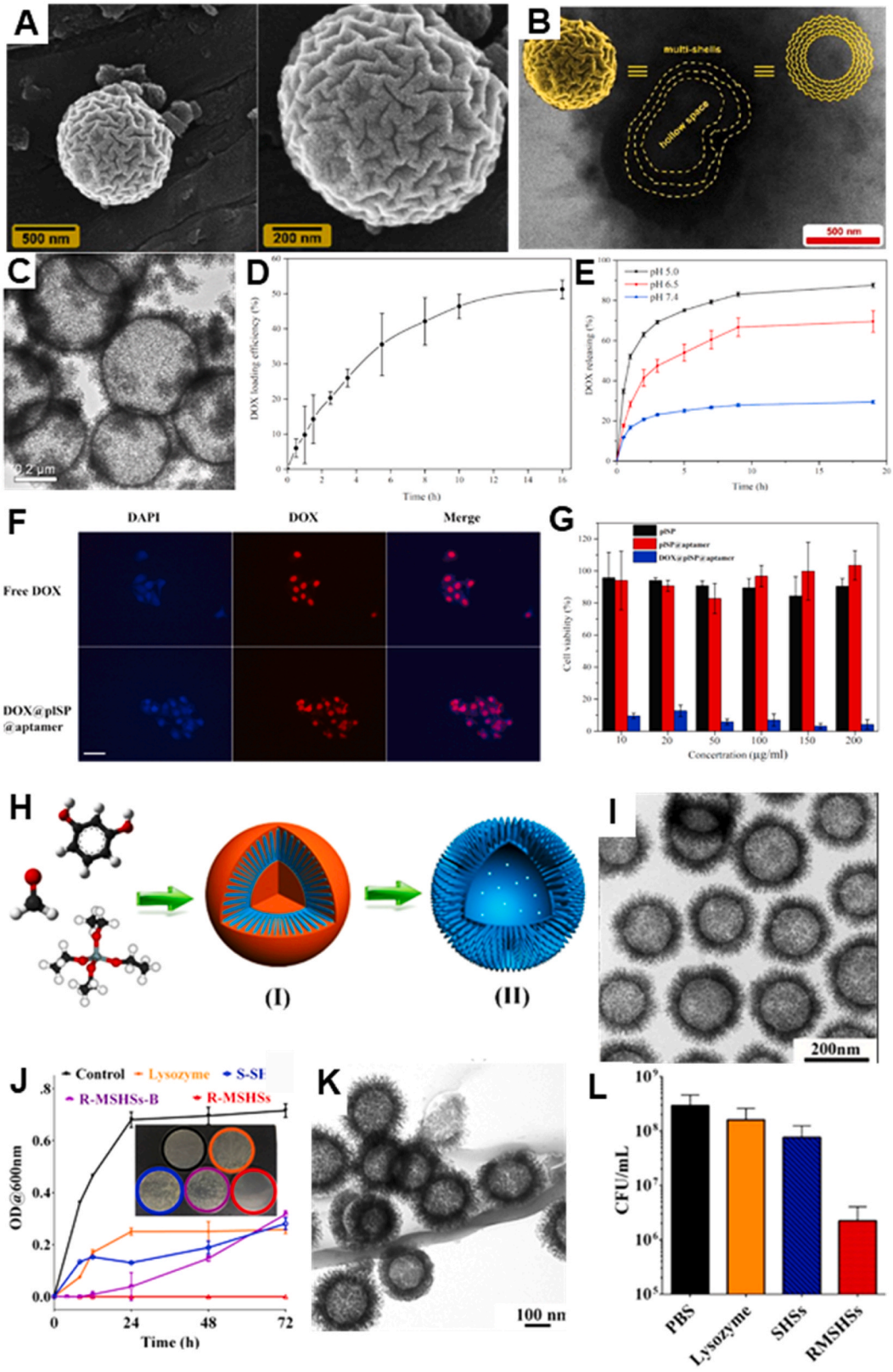

Fig. 4. Silica nanostructure. (A) SEM images of MI-PLMS. (B) TEM images of MI-PLMS[43]. (C) TEM images of pLSP@aptamer. (D) The drug encapsulation efficiency of plSP@aptamer. (E) The pH-triggered release patterns of DOX from the DOX@plSP@aptamer nano-carriers. (F) The fluorescent microscope images of MCF-7 cells. (G) The survival rate of MCF-7 cell incubated incubation with various nanoparticle[97]. (H) Schematic diagram of the synthesis of Silica Nano-pollens. (I) TEM images of R-MSHSs. (J) Time-dependent anti-bacterial efficacy of lysozyme in its free form compared to lysozyme encapsulated within silica nanospheres. (K) TEM images of *Escherichia coli* (*E. coli*) treated with R-MSHSs containing lysozyme for 24 hours. (L) *E. coli* that survived in the small intestine after treatment with silica nanopore loaded with lysozyme[29].

area and porous configuration, and it also holds potential for various biomedical applications. It underscores the significance of surface modification in mesoporous silica nanoparticles possessing high surface areas. Jin et al. synthesized aptamer-functionalized pollen-like hollow silica particles (pLSP@aptamer) using a unified one-pot strategy combined with glutaraldehyde crosslinking [97]. The fabricated pLSP@aptamer particles were encrusted with nano-scale protrusions mimicking the surface spikes of natural pollen (Fig. 4C). The extensive internal porosity and augmented surface area of the pLSP@aptamer played a pivotal role in achieving increased drug-loading efficiency (Fig. 4D). Additionally, the drug delivery platform exhibited pH responsiveness, attaining a maximum release efficacy of 87.5 % at pH 5 (Fig. 4E). The spike of the pLSP@aptamer functioned as an entry claw, facilitating attachment to the cell membrane and promoting enhanced nanoparticle-cell interactions (Fig. 4F). The pLSP@aptamer demonstrated potential as a tumor-specific therapy with effective drug delivery and low cytotoxicity (Fig. 4G). Another study reported that pollen-mimicking silica nanoparticles with improved bacterial adhesion [29]. As shown in Fig. 4H, the silica nanoparticles were synthesized by adding chemicals to the Stöber synthesis solution. The prepared rough mesoporous silica hollow sphere nanoparticles (R-MSHSs) exhibited consistent morphology and spiky surface (Fig. 4I). The R-MSHSs demonstrated higher bactericidal activity than the other nanoparticles over a prolonged period (Fig. 4J). This increased antibacterial efficacy was ascribed to the augmented adhesion of R-MSHS to the bacterial surface, which was facilitated by surface roughness. This enhanced adhesion allowed for effective

antibiotic delivery and subsequent lysis of the bacterial cell walls (Fig. 4K). Furthermore, R-MSHS exhibited superior *in vitro* antibacterial efficacy compared to the other experimental groups (Fig. 4L). These findings demonstrate that the characteristics of pollen structure significantly contribute to the sustained delivery of antibacterial agents and effective bacterial eradication. Table 1 summarizes a few notable pollen-inspired micro/nano carriers in biomedical applications.

Table 1
A few examples of the pollen-inspired micro/nano-carriers in biomedical applications.

Pollen source	Naturally/ chemically synthesized	Micro/ nano-carrier diameter	Applications	Ref.
Sunflower	Naturally	37.93 ± 1.41μm	Drug delivery	[98]
Lycopodium clavatum	Naturally	29μm	Living cell encapsulation	[99]
Dandelion	Naturally	27.46 ± 2.26μm	Candidate for: Drug delivery	[100]
Camellia sinensis, Sunflower, Baccharis halimifolia L, Rhus chinensis, Common poppy, Leonurus cardiaca, Nelumbo nucifera	Naturally	35–43μm	Candidate for: Drug delivery, actuators	[101]
Ambrosia elatior	Naturally	15–25 μm	Oral vaccine	[65]
Lycopodium clavatum	Naturally	25μm	Oral vaccine	[102]
Sunflower	ZnO	20–25μm	Selective detection application of NO2	[103]
Dimorphotheca-ecklonis	hybrid micro/ nanostructures Ag-Fe_3O_4	14.33 ± 5.28 nm	Improve the SERS (Surface-Enhanced Raman Scattering) activity.	[104]
Spike pollen	Metal-organic framework (MOF)	1–2μm	Antigen/ adjuvant-presenting particles for vaccination	[105]
—	Fe_3O_4 @$MgSiO_3$	210 nm	Highly effective capture of small extracellular vesicles	[106]

P-M/N bots with actuation

Micro/nanorobot actuation and strategic research have demonstrated that micro/nanorobots cannot transfer energy from standard batteries. Instead, their energy supply predominantly relies on chemical actuation, physical actuation, or a combination of both. The conversion of chemical energy into kinetic energy, usually via a chemical reaction, is a popular method of chemical actuation involving a pH reaction [35]. This is generally driven by the decomposition of peroxide to create bubbles [107,108]. However, because hydrogen peroxide is regarded as a toxic agent to the human body, it is not easy to use it inside the human body. Physical driving methods primarily include magnetic fields [109–112], light [113,114], and temperature [115,116]. Table 2 summarizes the materials and operation methods of stimulus-responsive micro/nanorobots in general.

Magnetic field responsive P-M/N bots

Magnetic fields are highly controlled, nonpolluting, and capable of penetrating biological tissues [122]. Magnetic fields can be used for several micro- and nanorobot functions because they can communicate as electrical impulses. In addition, its orientation and magnetization direction can be modified based on its application. Carmem et al. exploited the properties of sunflower pollen particles to develop a magnetically actuated microrobot by asymmetrically depositing a metal layer with magnetic capabilities (Fig. 5A-B). Sunflower pollen-based BioBot (SFPμP-BioBot) exhibited precise directional control in linear (Fig. 5C) and circular(Fig. 5D) as a result of actuation experiments under a transverse rotating magnetic field in a cell culture medium[123]. These findings illustrate the feasibility of magnetic actuation for the SFPμP-BioBot, enabling directed movement toward the intended target. Moreover, SFPμP-BioBot showed a remarkable ability to interact with and eliminate human ovarian cancer cells. Doxorubicin (DOX) exploited the electrostatic interaction between positively charged magnetic SFPμP-BioBot and negatively charged cancer cells to eradicate cancer cells without direct contact (Fig. 5E). In another study, a hybrid magnetic robot derived from chrysanthemum pollen has been reported [47]. Chrysanthemum pollen-derived biohybrid magnetic microrobots (CDBMRs) were fabricated by depositing magnetic nanoparticles (MNPs) onto chrysanthemum pollen using treated internal materials (Fig. 5F). A magnetic layer was produced with a portion of the exposed porous structure (Fig. 5G-H). These CDBMRs achieve various behaviors under different magnetic profiles (Fig. 5I-K).

Moreover, the interactions among CDBMRs can be harnessed to coordinate swarm control. A rotating magnetic field at $\delta = 0^\circ$ showed a swarm rotation mode, showing the possibility of fine mass transfer, while at $\delta = 90^\circ$, it showed a rolling propulsion toward a specific direction (Fig. 5L-M). Quantitative velocity measurements in PBS (Fig. 5 N) and DMEM (Fig. 5O) were performed to investigate the propulsion performance of the robot in its biological environment. At a magnetic field strength of 5mT, the translational speed increased with the magnetic frequency before reaching a critical frequency (21 Hz).

Furthermore, CDBMRs can be propelled at relatively high frequencies (>40 Hz) and speeds greater than 400 m/s, exhibiting exceptional magnetic response performance and significant potential for applications, such as ultrafast propulsion microrobots (Fig. 5O).

Magnetic field-driven P-M/N bots have shown remarkable precision

Table 2
Summary of materials and actuation of biochemical and physical stimulus-responsive micro/nanorobots [39].

Materials	Size (Shape)	Stimuli	Response/ task	Actuation input	Application	Ref
NIPAM/MNPs	— (round shape)	Temperature	Swelling/ shrinking drug release	Magnetic field	MRI system	[117]
Mg/Pt-NIPAM	50μm in diameter (spherical)	Temperature	Swelling/ shrinking drug release	Chemical	Controlled drug delivery	[118]
Gelatin/PVA/MNPs/ PLGA	100−250μm diameter (round)	Light (NIR 808 nm)	Photo-thermal targeted cancer therapy	Magnetic field	Targeting property and drug delivery	[119]
Mg/Au/ EUDRAGITU L100–55	20μm diameter (round)	pH	Acidic-induced protonation drug release	Chemical	Autonomous release of drug	[120]
EMK/AAc/ NIPAM/ DPEPA	60μm diameter (hollow sphere)	pH	Swelling/ shrinking grasping/ drug intake	—	Multi-functional compound micro-machines	[121]

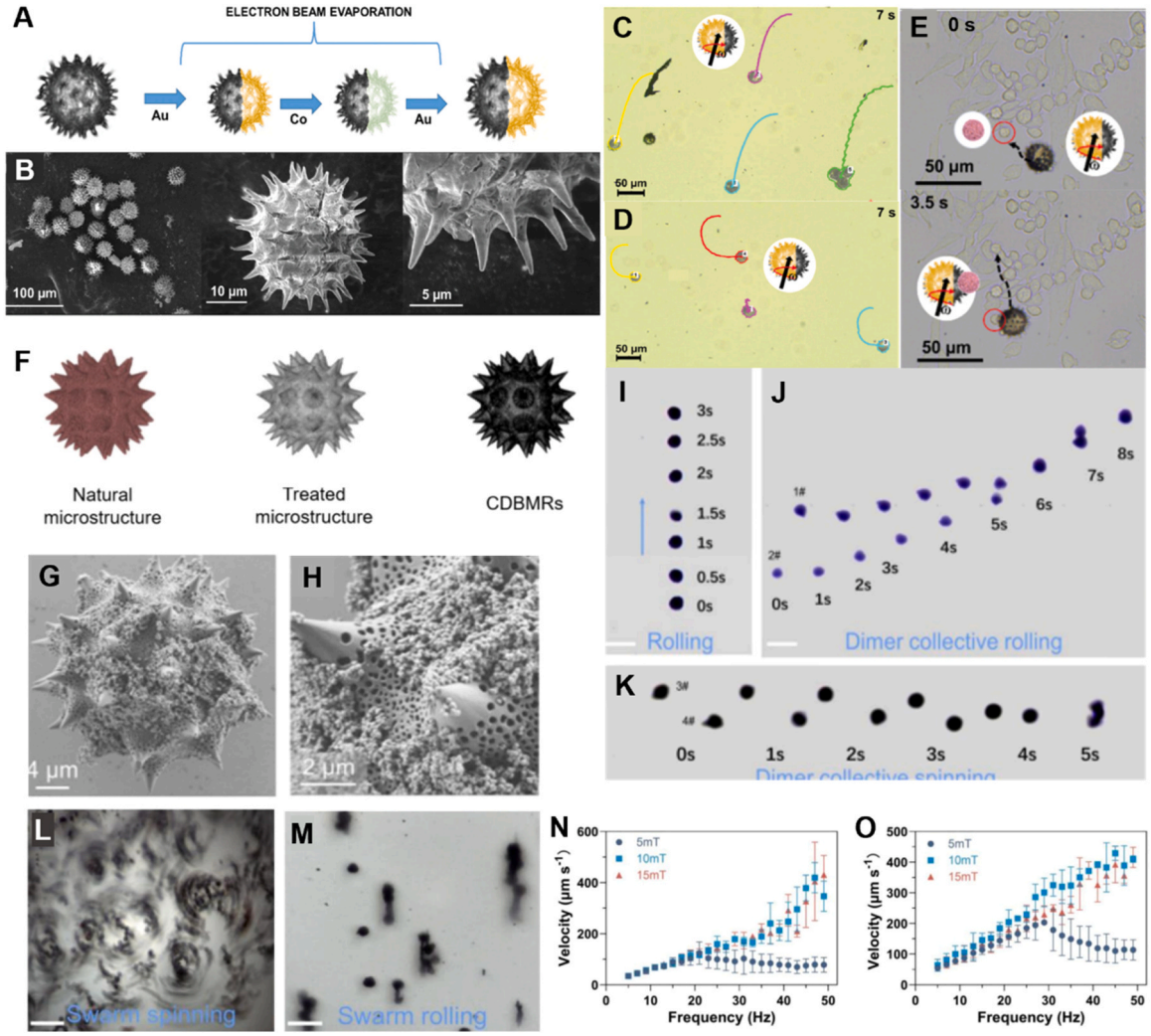

Fig. 5. (A) Schematic illustration of SFPμP-BioBot synthesis by magnetic particle asymmetric deposition of sunflower pollen microparticles. (B) SEM images of SFPμP-BioBot. Actuation of magnetic SFPμP-BioBots Linear (C), circular (D). (E) Time-lapse photographs show a magnetic SFP-BioBot attracting cancer cells and interacting with them[48]. (F) Schematic image of sequential manufacturing of CDBMR. (G) SEM image of CDBMRs. (H) Zoom-in image of CDBMRs's surface morphology. (I) Cyclical displacement of an individual Controlled Directional Brownian Magnetic Robot (CDBMR) in response to a revolving magnetic field (10mT, 5 Hertz). The arrow signifies the trajectory of motion. (J) Cooperative dynamics exhibited by dimerized CDBMRs through the rolling mechanism and (K) spinning mode. (L) Unified rotational motion exhibited by the swarm of CDBMR. (M) Collective rolling dynamics observed within the swarm of CDBMR. CDBMR translational velocity in (N) PBS and (O) DMEM(n=3) at various magnetic strengths [47].

in directional control and exceptional penetrability, proving to be highly effective for medical applications within dense tissues, such as cancerous cells. However, the use of magnetic micro/nanorobots in clinical settings requires compliance with stringent biocompatibility standards that many magnetic materials do not meet. Biocompatible magnetic materials, such as superparamagnetic iron oxide

nanoparticles, are currently employed; however, their relatively weak magnetization constrains the effectiveness of magnetic manipulation in micro/nano robots[124]. Consequently, there is a need for additional research on magnetic materials that offer strong magnetization and demonstrate long-term biocompatibility.

Light-responsive P-M/N bots

Light is an appealing energy source for driving the movements of micro/nanorobots and motors because of its remote-control capabilities, high spatiotemporal resolution, and highly adjustable output (amplitude, frequency, and path of propagation) [125]. Light-induced phoresis, light-induced bubble recoil, light-induced interfacial tension gradients, and light-induced deformation are the few propulsion mechanisms that have been hypothesized and realized to date [126]. UV-responsive nanorobots are toxic to the human skin and have a low tissue penetration depth. In contrast, NIR-responsive robots are considered essential because they penetrate deep into the tissues [127, 128]. Song et al. designed and fabricated a light-controlled spike motor based on polydopamine-functionalized sunflower pollen by introducing synergistic topographic interactions (Fig. 6A) [129]. Sunflower pollen grains (SPGs) and formaldehyde (FA)/SPG had smooth surfaces, but polydopamine (PDA)/SPG had a rough surface owing to the PDA coating (Fig. 6B-ii). As illustrated in Fig. 6C, the micromotor was driven and adjusted by changing the laser beam power density and irradiation direction, demonstrating the trajectories under various laser power densities when the laser was irradiated near the micromotors, initially approaching the laser focus point before bouncing back and moving in the opposite direction (Fig. 6D). The number of yeast cells captured by 3-aminophenylboronic acid (APBA)/PDA/SPG micromotors was approximately six times higher than that captured by the PDA/SPG micromotors (Fig. 6E). These observations indicate that both APBA and its pointed configuration play important roles in the preferential capture of yeast cells by micromotors. In another study, near-infrared II (NIR--II)-activated micromotors for treating inflammatory bowel disease (IBD) were fabricated by asymmetric doping of Au layers on sunflower pollen particles[37]. The micromotor was driven by the thermophoresis effect of NIR (Fig. 6**F-G**). The temperature of the micromotor was found to correlate with the wavelength and intensity of the NIR light, along with the duration of doping of the Au layer **(**Fig. 6**H-J)**.

Moreover, the micromotors revealed that when subjected to consistent power levels and a uniform Au layer thickness, the temperatures were higher with NIR-II irradiation than with NIR-I irradiation (Fig. 6K-L). The velocity of the micromotor increased with the Au layer thickness and NIR-II irradiation power (Fig. 6M). These results indicate that pollen-derived micromotors can serve as promising conveyors for various clinical applications when actuated by NIR-II. Micro/nanorobots that use light can accelerate the rapid formation of micro/nanorobot swarms by leveraging positive phototactic movements, thereby allowing accurate control. Moreover, the heat produced by light can be used in various therapeutic applications. However, the heat produced by light activation can lead to significant biological harm and tissue damage [130–132], potentially resulting in irreversible injury to living tissues or organs[133,134].

Temperature-responsive P-M/N bots

Temperature-sensitive materials have been used to construct thermo-responsive micro/nanorobots. pNIPAM is a typical example of a temperature-responsive micro/nanorobot [116–118,135,136]. The most widely used thermosensitive hydrogel is pNIPAM, which has a critical solution temperature (LCST) near body temperature. The hydrogen bonds in pNIPAM were disrupted above the LCST, resulting in an aqueous contractible conformation. pNIPAM-based micro/-nanorobots are employed for drug delivery because of their ability to alter their morphological characteristics or physical topology in response to surrounding temperature changes[117,137]. A hydrogel micro/nanorobot using pNIPAM(was fabricated using a photonic 3d laser printing protocol [138]. The shell shrank as the temperature increased from 25 to 45 °C (Fig. 7B). The multifunctional pollen grain-inspired hydrogel micro/nanorobot (MPH) robot had two modes that could be selected based on the temperature of the outer shell (Fig. 7A). The robot can be attached to a target place in the attachment mode, which reveals the outer shell's spikes, and it can roll on a surface in the locomotion mode, which keeps the outer shell's spikes hidden (Fig. 8C-D). These shape changes are repeated without any change in quality. The spike structure improves the pulling force and friction against the pig intestines compared to the round structure (Fig. 8E). Spike structures generate higher pulling and friction forces than round structures because surfaces, such as soft tissue, allow spikes to penetrate (Fig. 8F). Thermoresponsive hydrogel-based micro/nanorobots utilizing pNIPAM can react with targeted temperature shifts, allowing them to be employed in drug delivery applications. However, pNIPAM hydrogels exhibit a slower expansion rate than their rapid contraction rates [139].

Furthermore, thermoresponsive hydrogels typically have lower mechanical strength than other types of hydrogels. Therefore, further research is needed to investigate hydrogels that can effectively revert from a dehydrated state to a swollen state while improving their mechanical strength.

pH-responsive P-M/N bots

Microorganisms in the natural world exhibit stress reactions in response to continuously fluctuating conditions, such as oxygen, pH, magnetic fields, and light intensity. Additionally, because the pH values of various biological components of the human body vary, these environmental changes provide specific conditions for site-specific treatment using pH-responsive nanocarriers [140–142]. Consequently, microrobots that sense their surroundings can distribute various types of medications [143]. Cai et al. developed a pH-responsive pollen-derived micromotor for the treatment of gastric ulcers [44]. The micromotor was fabricated by asymmetrically doping a Mg layer on one side of the herbal medicine pollen (Fig. 8A). Only one side of the sporopollenin exine capsules (SECs) was covered with an Mg layer, while the other side maintained its spine-like shape, resulting in almost no damage to the structure of the SEC (Fig. 8B). The magnesium layer combined with hydrogen ions in the presence of gastric juice, producing hydrogen bubbles that powered the micromotor (Fig. 8C). As the pH value increased, the H^+ concentration decreased, thereby reducing the generation of bubbles and the average speed of the micromotor. The speed of the micromotor increased as the thickness of the Mg layer increased, owing to the Mg/H^+ reaction (Fig. 8D). IL-10 inhibited inflammation by decreasing the expression of several inflammatory factors. IL-10 expression increased after gavage with a micromotor containing berberine hydrochloride (Fig. 8E). Pollen-derived micromotors move autonomously in the stomach and attach to the surrounding tissue to extend residence time. Pollen-derived micromotors show excellent adhesion and gastric ulcer treatment efficacy. pH-sensitive micro/-nanorobots can be engineered to function exclusively at specific pH levels, ensuring that they operate only under designated conditions, thereby allowing precise control. However, as the pH can be influenced by various factors, it is challenging for micro/nanorobots to accurately detect the exact pH and respond accordingly.

Therapeutic applications

Micro/nanorobots can perform tasks in a minimally invasive manner and have significant potential in the biomedical field owing to their high bio-adhesion and structural advantages. A further improved target-delivery effect can be achieved using stimulus-responsive materials in these spike micro/nanorobots. This section describes improved treatments using pollen inspired-structured micro/nanorobots. Table 3

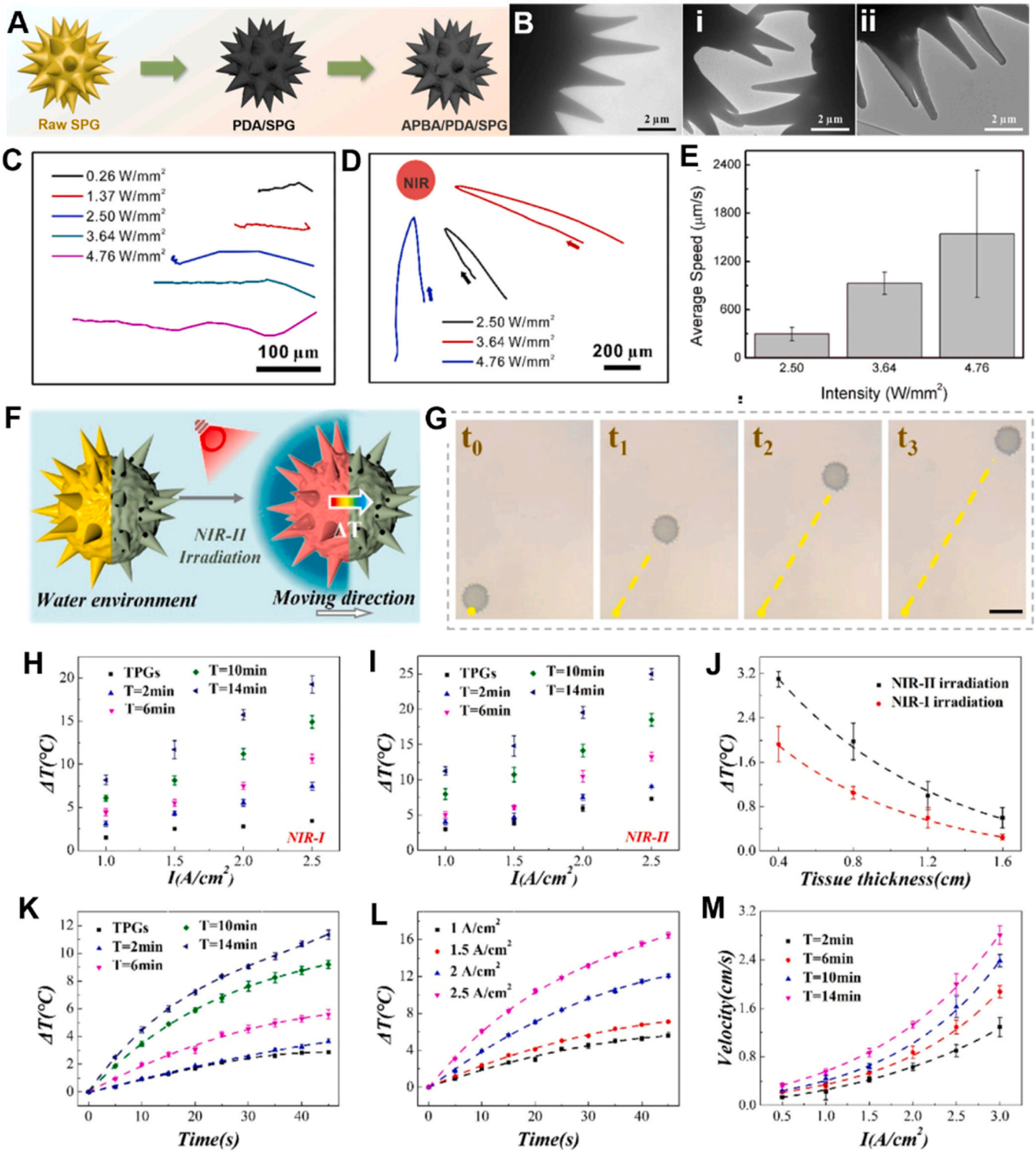

Fig. 6. (A) Schematic diagram of pollen-inspired micromotor fabrication. TEM images of the raw SPG (B), FA/SPG (i), and PDA/SPG (ii). (C) The average speed of the micromotor at various laser power densities. (D) Round-trip trajectory in under 1 second. (E) The correlation between the mean velocity of the microscale motor under varying power densities of NIR laser[129]. (F) Diagram depicting the autonomous propulsion mechanism of Photothermal. Driven Microscale Machines (PDMMs). (G) The locomotion pattern exhibited by PDMMs when subjected to NIR-II irradiation. (H) Temperature variation for PDMMs with different durations of Au sputtering at different power levels of NIR-I irradiation. (I) Temperature fluctuations in PDMMs with distinct durations of Au sputtering under varied power levels during NIR-II irradiation. (J) Temperature evolution for PDMMs with Au sputtering time of 14 min under NIR-II irradiation through textures of various thicknesses. (K) Temperature variation for PDMMs with distinct durations of Au sputtering under NIR-II irradiation conditions. (L) Speed of PDMMs with varied durations of Au sputtering under diverse power levels during NIR-II irradiation. (M) Speed of PDMMs with varying durations of gold sputtering, subjected to different intensities of NIR-II irradiation [37].

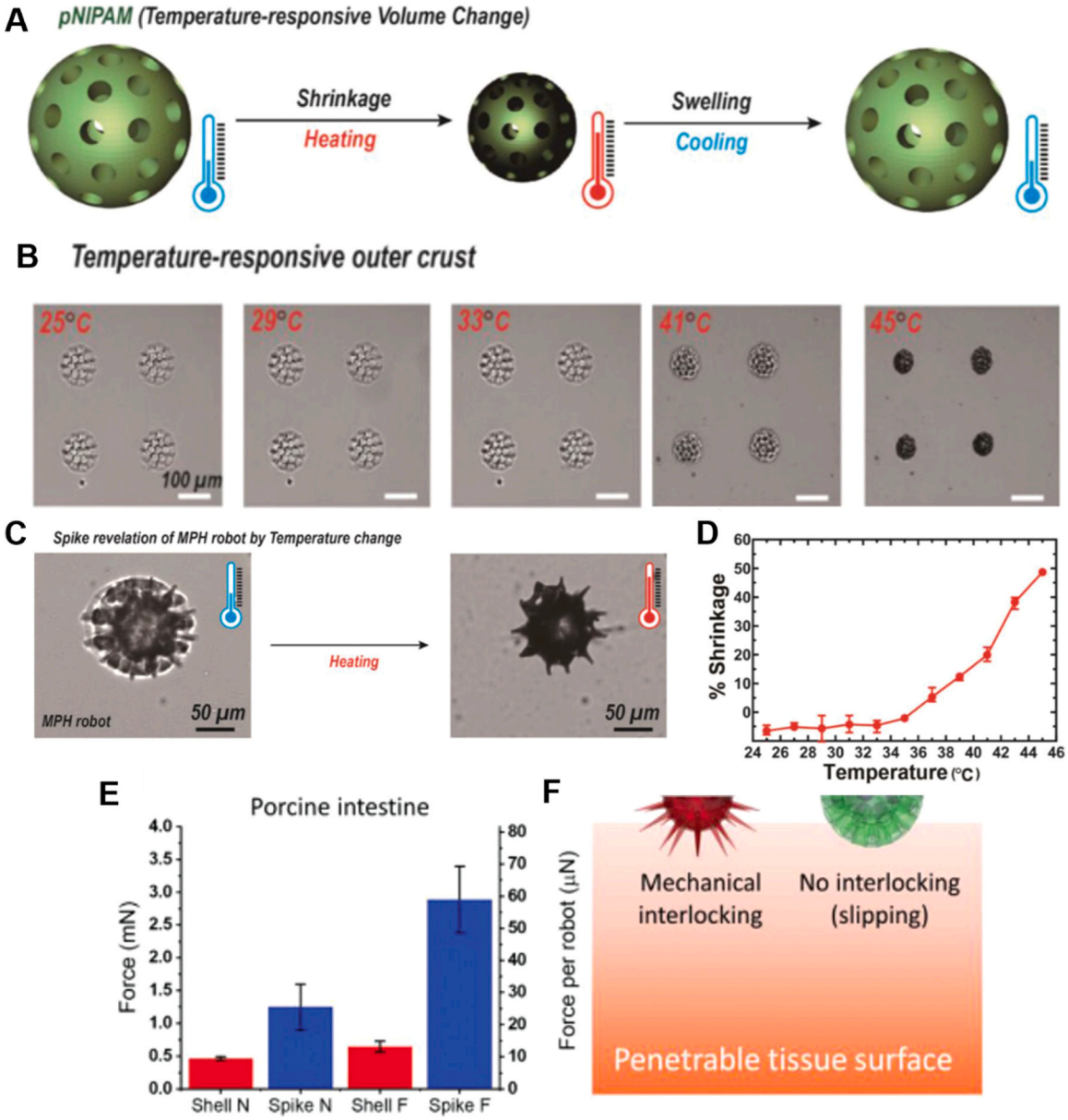

Fig. 7. (A) Diagrammatic representations depicting the contraction of the external layer of the MPH robot induced by temperature changes. (B) microscopic pictures demonstrating how the pNIPAM hydrogel's outer shell structure shrinks in response to temperature variations (25–45°C). (C) Micrograph of the spike structure of the MPH robot in response to temperature. (D) Shrinkage ratio with increasing temperature of pNIPAM hydrogel. (E) The forces exerted by each robot, with a spherical and spiked frame, against the intestines of pigs. (F) Schematic diagram of attachment of spikes and shells to soft tissue [46].

summarizes key benefits of microrobots compared to the existing methods of therapeutic applications.

Drug delivery system

Nanocarriers with the capability of targeted drug delivery and controlled release play a pivotal role in optimizing treatment efficiency by minimizing drug consumption and mitigating side effects [151]. Currently, sustained and regulated drug release is attainable through factors, such as temperature [152], pH [153], light [154], and magnetic sensitivity [155]. Exine capsules derived from pollen have shown promise as a delivery mechanism for a range of drugs [50,156–162]. The hollow structure and high surface area of pollen allow sustained drug release via mucoadhesion and cell adhesion [163,164]. (Fig. 9A). Maric et al. evaluated the drug delivery potential of microrobots derived from the pollen of nine different species [64]. In the DOX loading and release experiment conducted on lotus pollen (Pt-Lot) with a large surface area as a representative of the Pt-microrobots, DOX was successfully loaded onto the microrobots (Fig. 9B-E). Moreover, the Pt-Lot microrobot exhibited targeted efficacy in delivering DOX, resulting in a 41 % reduction in cell viability of the MCF-7 cell line. (Fig. 9F Magnetic guidance using permanent magnets can directly target drugs within alternating magnetic field systems. Furthermore, the application of an alternating magnetic field induces a temperature increase that controls the drug release. Cai et al. developed dandelion pollen-inspired $CoFe_2O_4$ porous microspheres with controlled drug release via atomic force microscopy [49]. The microspheres were created using a 3D hierarchical approach devoid of templates. The resulting microspheres exhibited significant porosity and nanoscale building blocks (Fig. 9G). Moreover, the microspheres exhibited robust magnetic responsiveness to magnetic fields and demonstrated the capacity for magnetic induction through the remote application of a magnetic field (Fig. 9H). The microspheres

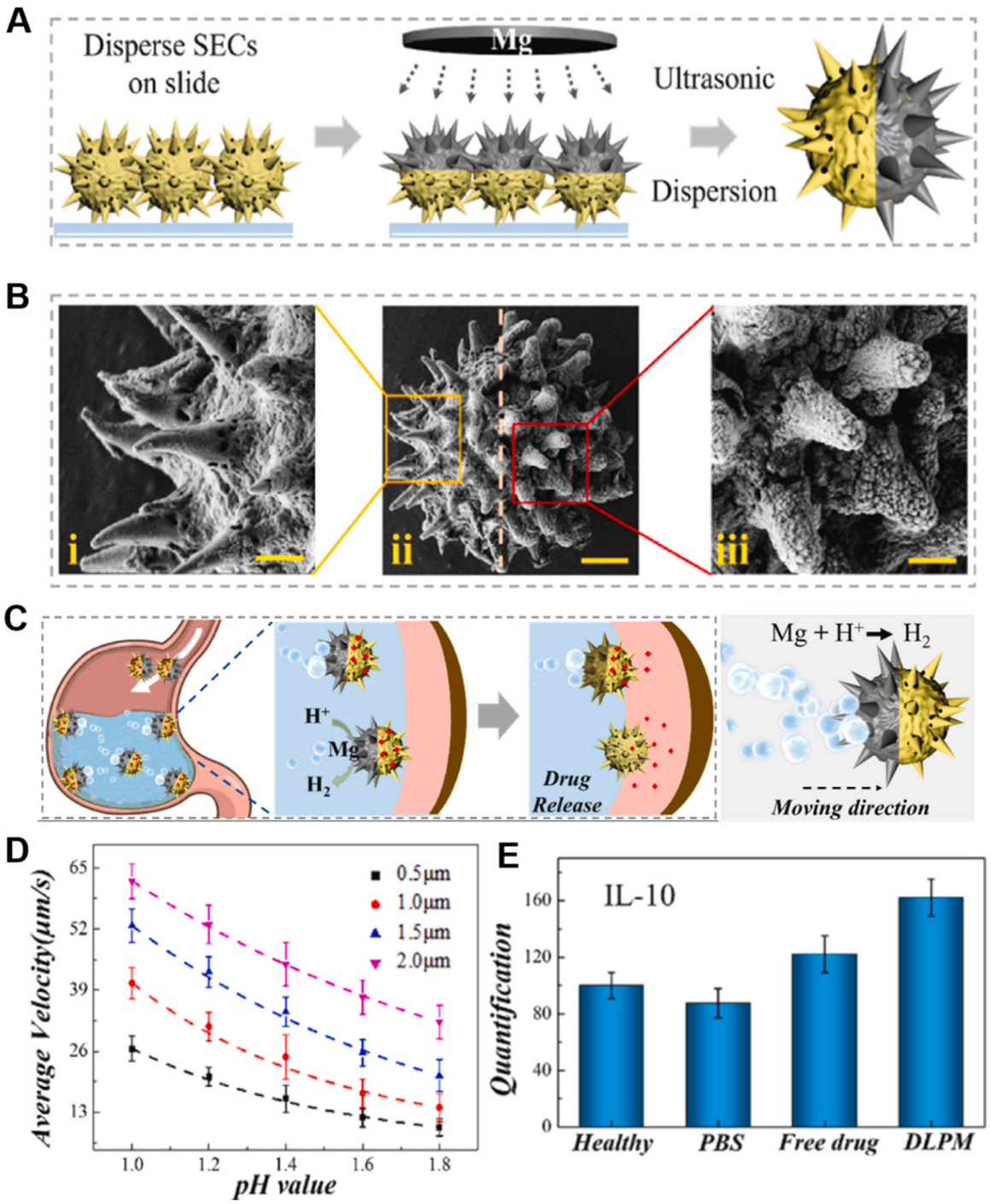

Fig. 8. Manufacture of pollen-derived micromotors. (A) Schematic diagram of pollen-derived micromotor fabrication. (B) SEM images of the undoped side of the pollen-derived micromotor (i), the overall view of the pollen-derived micromotor (ii), and the Mg-doped side (iii) of the pollen-derived micromotor. (C) Autonomous movement mechanisms of pollen-derived micromotors. (D) Statistical analysis of the average speed of pollen-derived micromotors at different pH values and Mg thickness. (E) Statistical analysis of IL-10 expression [44].

exhibited excellent drug-loading ability (Fig. 9I). Under the influence of an alternating current magnetic field, the microspheres exhibited sustained drug release at high frequencies and magnetic field strengths (Fig. 9J-L). These result underscore the capability of porous microspheres to execute controlled drug release processes, establishing them as promising structures for applications in drug encapsulation and controlled drug release.

Anti-cancer therapy

Cancer treatment has significantly improved in the last few decades [148,165,166]. However, it remains impossible to deliver the optimal therapeutic concentration of anti-cancer drugs to the target site using standard treatments[167]. Progress in pollen-inspired structure micro/nanorobots holds significant promise in addressing diverse obstacles related to drug targeting and delivery[168–170]. In recent years, there has been significant interest in NIR-triggered photothermal therapy (PTT) owing to its minimally invasive approach for precisely

Table 3
Benefits of microrobots compared to existing treatment methods for biomedical applications.

Biomedical application	Existing approaches	Pros/Cons	Micro/nanobots advantage
Drug delivery	Extracellular vesicles (Ev) [144], nanoparticle based delivery [145]	High drug loading /less target-specific	High target specific [146]
Wound healing	Hydrogel [147]	Maintains moist wound environment /risk of infection	Treatment of deep wounds [36,44]
	Semipermeable film [147]	Maintains moist wound environment /aids bacterial overgrowth in the moist environment	
	Contact layer [147]	Low adherence/ permeable to bacteria	
Cancer therapeutic	Gene therapy, Stem cell therapy [148]	Safe and effective/ Potential tumorigenesis Expression of proapoptotic/ high chances of being neutralized by the immune system	High controllability, Deep tumor penetration, and Cell internalization [47,149]
Bacteria therapeutic	Antibiotic [150]	Antibiotic resistance	Antibiotic Resistance is Prevented, effective biofilm removal [45]

targeting tumors without harming adjacent healthy tissues[171–173]. PTT absorbs NIR light and converts it into heat, which destroys cancer cells through thermal ablation. PTT formulations containing heavy metal components exhibit high photothermal conversion efficiency but have serious safety concerns[174]. Hollow SECs have been reported as safe and uniform size and composition[175]. As shown in (Fig. 10A), sunflower SECs showed improved photothermal efficacy compared with the other SECs. In this regard, SECs show an increased photothermal response in nanoparticles with spiked structures[176]. Moreover, a rapid increase in temperature was observed in tumors exposed to sunflower SECs, whereas saline-treated tumors showed only a minimal increase in temperature. As shown in (Fig. 10B), the growth of tumors treated with SEC employing NIR was significantly prevented by this effective temperature increase. Another study engineered a micro/nan robot with spike features capable of reaching tumor cell tissue, even in the rigid stroma and connective tissue resulting from tumor growth [177]. Owing to the extensive fibrotic connective tissue and dense extracellular matrix in triple-negative breast cancer, nanorobots face significant challenges in reaching the tumor and penetrating the cells to deliver anticancer drugs. Urchin head/hollow tail nanostructures (UHHTNs) comprise NIR-absorbing Au nanospike partially covered with a silica shell in the head section, with a hollow tail connected to the semi-coating. UHHTNs can easily penetrate tumors by strongly binding to cell membranes using its pointed head and hollow tail with a dedicated opening (Fig. 10C). Tumor photothermal therapy was also achievable because of the AuNPs in UHHTN. The temperature of UHHTN aqueous solution (concentration 100 μg/mL), which increased with increasing concentration of UHHTN under laser irradiation, demonstrated the photothermal function of the nanorobot (Fig. 10D). DOX for tumor treatment was effectively loaded into UHHTN and released at various laser power densities (Fig. 10E). Motion analysis to ascertain the controllability of the nanorobot revealed a progressive increase in the mean square displacement over time across various NIR power densities (Fig. 10F). These manipulable spike robots require the capability to breach cell membranes to facilitate tumor treatment. MDA-MB-231 cells were subjected to laser treatment with either spikeless or spiked particles. The confocal laser results demonstrated a notably higher cellular absorption rate for the spiked particles than for their non-spiked counterparts, indicating that their proficiency in breaching the cell membrane was visibly evident (Fig. 10G). In the tumor treatment experiment, the UHHTN/DOX+laser group demonstrated diminished tumor sizes in the spinal region compared to the remaining groups, as depicted in Fig. 10H. In summary, the UHHTN/-DOX+laser combination notably suppressed tumor progression, as indicated by the measurements of tumor weight and volume (Fig. 10I-J). Xu et al. developed a magneto-optic driven spike nanomachine[178]. The nanomachine utilizes a magnetic core composed of zinc-doped iron-oxide nanoparticles and Au nanotips, exhibiting magneto-optical coupling in the NIR-II spectrum. This was effectively driven towards cellular lysosomes through controlled viscosity regulation by thermal means, demonstrating cancer cell destruction *in vitro* and *in vivo*. The unique chrysanthemum pollen grains make it ideal for self-regulating medicinal applications. Large pores, barbed protrusions, and porous structures used for cargo encapsulation and transport increase the surface roughness, facilitating adhesion. Considering these characteristics, a CDBMR was developed for tumor treatment[47]. To illustrate the targeted intervention of tumor cells through dynamic magnetic manipulation, micromotors loaded with magnetic drugs derived from chrysanthemums (CDMDP) were guided toward live HeLa cells using feedback from confocal laser scanning microscopy images (Fig. 10 K). CDMDP exhibited red autofluorescence, which served as a real-time indicator of magnetic control. HeLa cells displayed green fluorescence, indicating their viability before perforation. CDMDP also harnessed a large internal chamber, demonstrating ample capacity for drug loading. DOX was incorporated into CDMDP via vacuum infiltration to yield CDMDP@DOX. As the dosage of CDMDP@DOX increased, there was a corresponding increase in the number of deceased HELA cancer cells (Fig. 10 L). These results demonstrate the effectiveness of tumor treatment with CDMDP by controlled drug release.

Anti-bacterial therapy

Nano-structured anti-bacterial surfaces can function synergistically with antibiotics to increase their efficacy against resistant bacteria [180–183]. Spike-shaped nanoparticles induce bacterial death by rupturing the bacterial membrane and subsequent cell lysis[184–186]. Remarkably, it does not exhibit toxicity towards mammalian cells[187]. Because they are larger than nanoparticles, mammalian cells can endure stresses that lead to bacterial membrane rupture. By enhancing spiked-particle micro/nanorobots with photothermal functionalities, a range of versatile antibacterial micro/nanorobots have been successfully developed [45]. The photothermal impact of micro/nanorobots also facilitates disinfection through elevated temperatures[112,188]. Photothermally-driven microrobots are created through the self-polymerization of dopamine hydrochloride (DA·HCl) on the carbonized SPG surface. The SPG structure retained its morphology after PDA conversion and carbonization. The range of movement of the microrobot expanded as the power intensity of the manufactured microrobot increased (Fig. 11A). Furthermore, manipulating the movement of microrobots is crucial because it defines their practicality. By regulating the NIR irradiation duration and placement, one can observe the transformation of the microrobot path into diverse patterns, such as a rectangle (Fig. 11B) and a spiral (Fig. 11 C). Fig. 11D illustrates the attainment of the PDA/SPG microrobot under laser exposure. The collection area of the PDA/SPG microbots expanded with increasing laser irradiation time (Fig. 11E). Microrobots gathered at a specific location in this manner have been employed for bacterial eradication by leveraging the localized heat produced by the photothermal

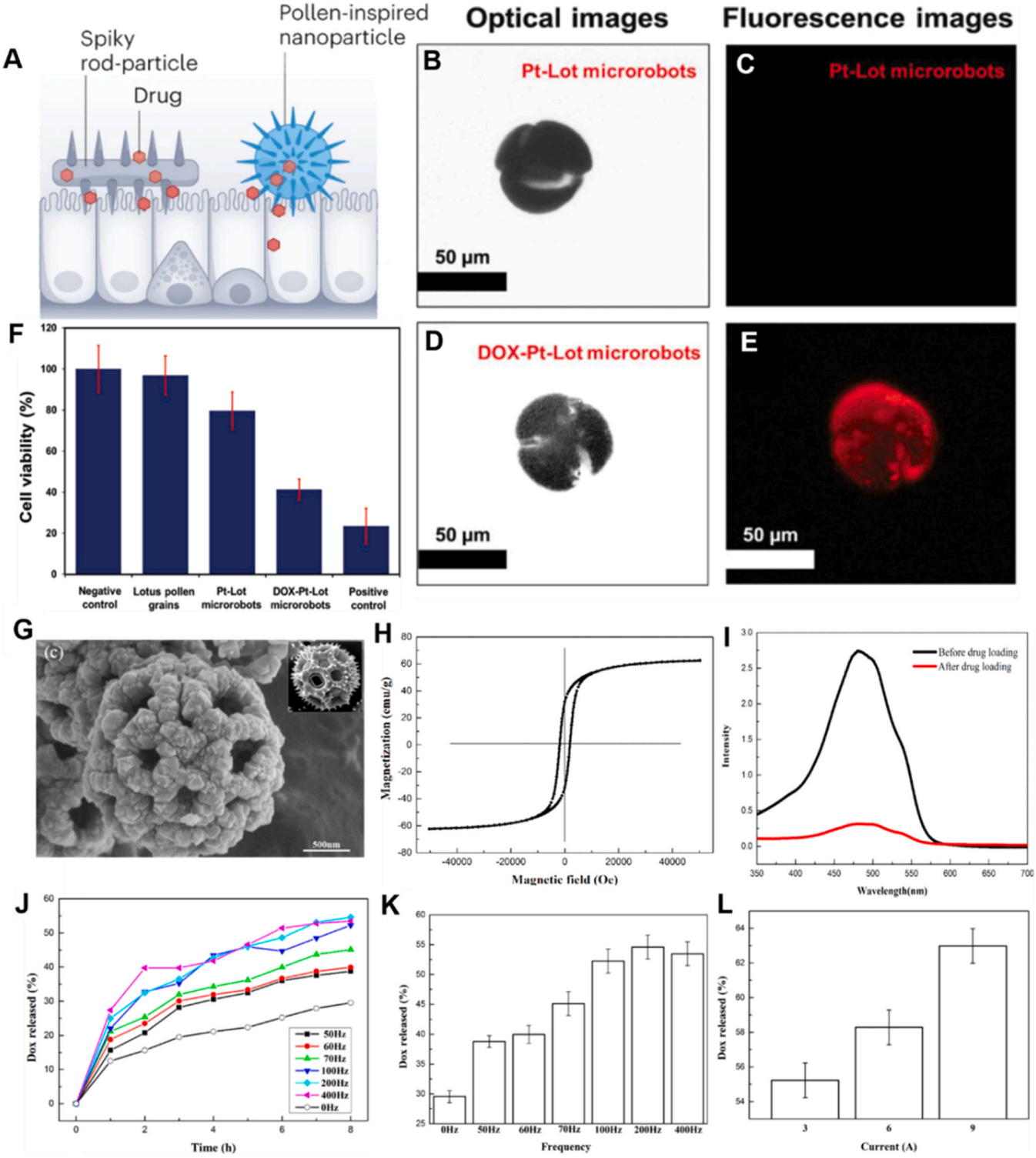

Fig. 9. (A) Bio-adhesion and sustained drug release of pollen-inspired nanoparticles. (B) Optical (C) Fluorescence images of Pt robot. (D) Optical (E) Fluorescence images of DOX-Pt-Lot robot. (F) Cell viability results of MCF-7 cells (WST-8 assay). Fluorescence images of the colon of mice were administered[64]. (G) SEM images of the $CoFe_2O_4$ porous microspheres. Inset: image of dandelion pollen grains. (H) Magnetization curve of the $CoFe_2O_4$ microspheres. (I) UV–vis absorption spectra of DOX solution before and after loading into microspheres. Magnetically controlled DOX release at different frequencies (J and K) and intensity (L)[49].

phenomenon. The microbot advanced towards the focal point during laser exposure and depicted the photothermally triggered disinfection procedure for *Staphylococcus aureus* (Fig. 11 F) and *E. coli* (Fig. 11 G).

Inflammatory gastrointestinal disease therapy

IBD is a prevalent gastrointestinal disorder with a significant occurrence distinguished by persistent inflammation that affects the colonic mucosa [189–191]. Given that IBD predominantly affects the colon, there is considerable clinical need for drug delivery systems that

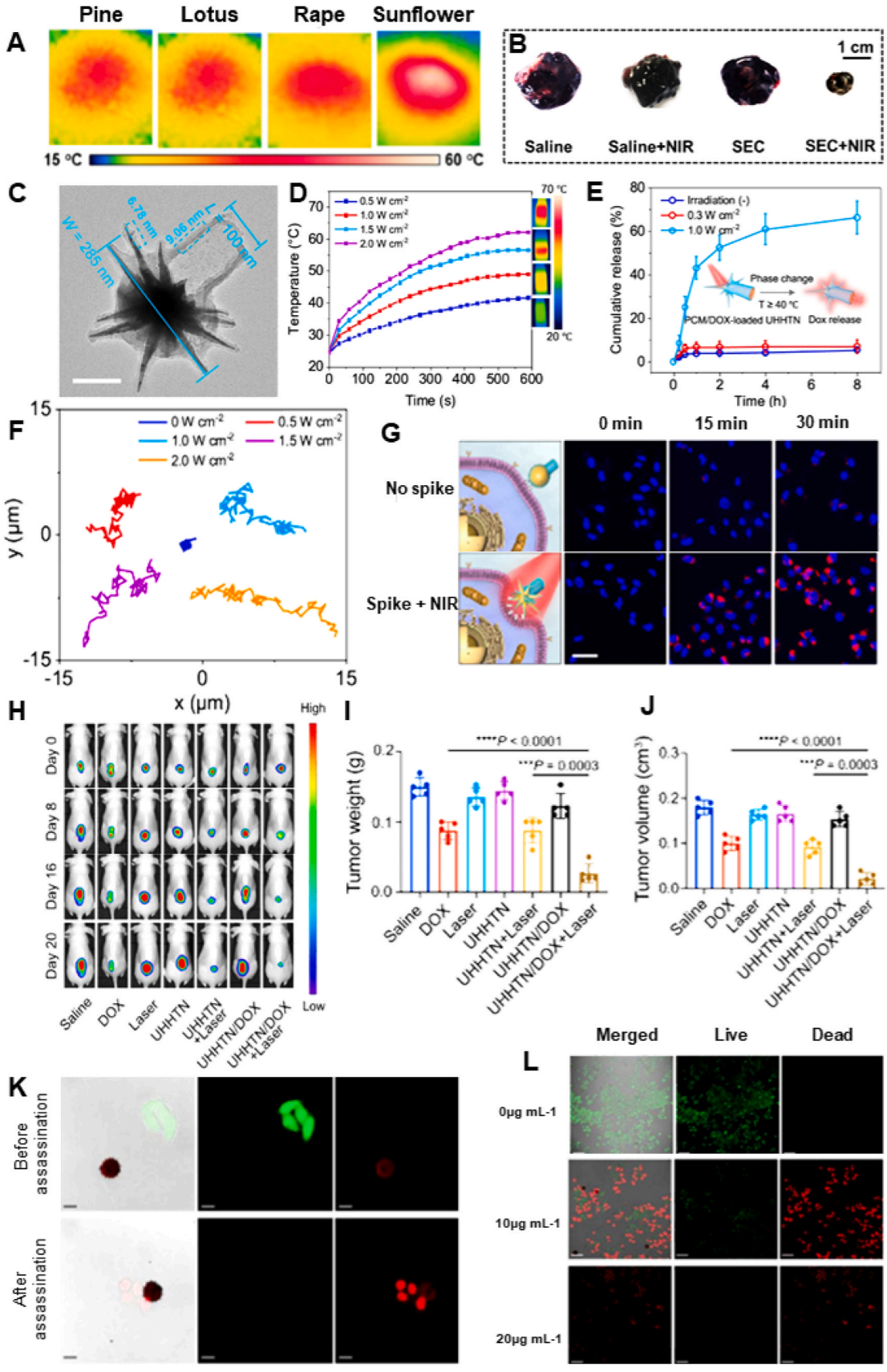

(caption on next page)

Fig. 10. **(A)** Photothermal images of various pollen. (B) Images of tumors after applying different treatment regimens[175]. (C) Enlarged TEM image displaying a solitary UHHTN with distinct surface protrusions. (D) Illustration depicting the thermophoresis mechanism. Upon local absorption of NIR light on one facet of a UHHTN, a temperature gradient emerges across the surface of the UHHTN. (E) Drug release profiles of DOX from the UHHTNs in DMEM. (F) Paths of PCM/nanorobots exposed to various NIR power intensities for 10 seconds. (G) Fluorescence images of MDA-MB-231 cells subjected to nanoparticles without nanospikes and nanoparticles with spikes at 0, 15, and 30 min. (H) Bioluminescence images at various time intervals following a 20-day treatment period in multiple cohorts of tumor-bearing mice. (I) Mass and (J) dimensions of tumors in immune-deficient mice with TNBC spinal metastases following diverse 20-day treatments using DOX [179]. (K) Combined and separated pathways within CLSM visuals capturing CDMDPs alongside HeLa cells, both stained for vitality (live/dead), pre and post intervention. The green and red emissions signify viable and non-viable cells, respectively. (L) Viability staining outcomes of HeLa cells cultured for 24 hours post-treatment with varying concentrations of CDMDPs[47].

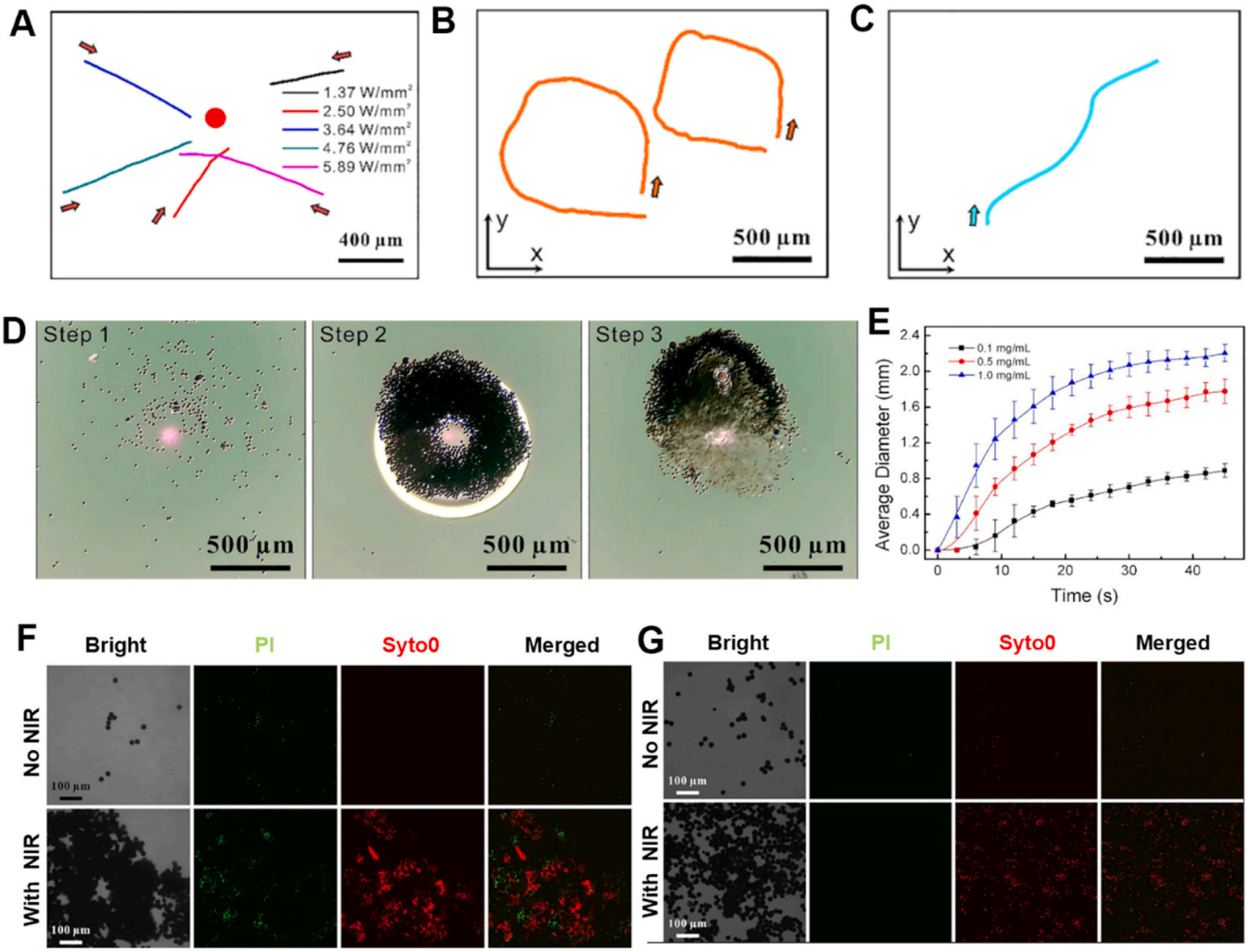

Fig. 11. **(A)** Movement paths over a 7-second duration. Regulate the movement direction by aligning the light spot position based on the laser intensity. **(B)** Rectangular configuration, **(C)** Spiral arrangement. **(D)** Aggregation process of PDA/SPG microbots under laser intensity. **(E)** Diameter of clusters after gathering various concentrations of microbots at laser intensity. **(F)** Anti-bacterial impact of microbots on *S. aureus* with and without laser under laser strength. **(G)** Anti-bacterial impact of microbots on *E. coli* with and without laser[45].

specifically target this region. Furthermore, because IBD is a chronic and incurable condition, the treatment objective is to achieve sustained relief and minimize drug side effects by delivering medications directly to the inflamed tissues[192]. The key challenge in devising drug delivery systems for IBD is the dynamic and diverse environmental conditions throughout the gastrointestinal tract[193]. Consequently, it is crucial to consider the stability of drug delivery systems influenced by enzymes found in the gastrointestinal tract. A micromotor derived from pollen activated by NIR has been reportedly designed to treat IBD efficiently [37]. The hollow structure and porous pollen surface contribute to its significant cargo-loading capacity, enabling effective drug delivery for the treatment of IBDs. The micromotor was fabricated through the asymmetric sputtering of Au layer on sunflower pollen and driven by thermophoresis. Fig. 12A shows a schematic diagram of the pollen micromotor driven by NIR-II to address IBD. The spike structure of the micromotor enables efficient attachment to the colonic tissue, thereby prolonging its residence time in the colon and enhancing drug delivery. Upon administering enemas containing spherical particles and micromotors to mice with IBD, a robust fluorescence signal was observed at the distal end of the colon after 1 h for spherical particles, with a diminished signal after 3 h. In contrast, mice that received a micromotor enema exhibited a persistent and strong fluorescence signal in the colon for up to 6 h. These results highlight the superior drug delivery efficacy of micromotors compared to that of conventional spherical particles (Fig. 12B-D). Furthermore, the micromotor was attached to the colon wall via a barbed structure, prolonging its residence time *in vivo*

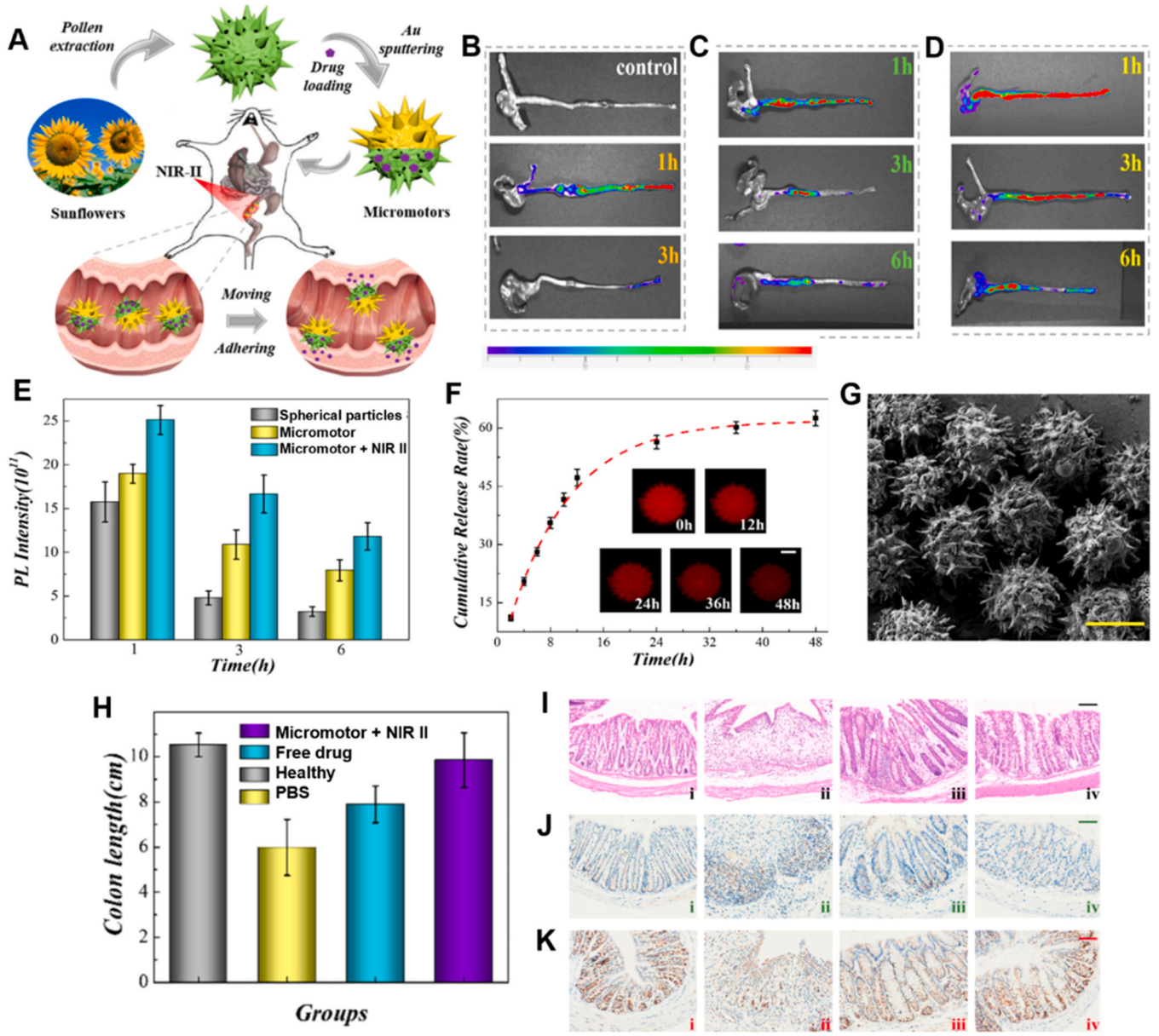

Fig. 12. **(A)** Illustration depicting pollen micromotors propelled by NIR II for the treatment of inflammatory bowel disease. **(B)** PBS (control) **(C)** micromotor **(D)** NIR II activated micromotor enema for 1 and 3 h. **(E)** Statistical evaluation of the *in vivo* adhesion test's fluorescence signal. **(F)** Accumulated release pattern of RhB-loaded micro motors. **(G)** SEM images of the micromotor retrieved from the colon; scale bar: 20 μm. **(H)** Statistical examination of the mice's colon length. **(I)** H&E staining and **(J)** Representative images of IL-1β and **(K)** ZO-1 activity of colons from healthy mice[37].

(Fig. 12E) and promoting gradual drug release over a long period (Fig. 12 F). The *in vivo* micromotor, with prolonged existence, showed stability by maintaining its original shape even 48 h after delivery to the colon (Fig. 12 G). Consequently, as illustrated in Fig. 12H, among the different experimental groups, the colon length of the micromotor-treated group closely resembled that of the healthy group, indicating effective therapeutic outcomes. Moreover, the H&E images of the colon tissue revealed reduced inflammatory cell infiltration and rarer epithelial cell detachment in the micromotor-treated group than in the other experimental groups (Fig. 12I). Moreover, the micromotor-treated group exhibited the lowest expression levels of key inflammation-regulating factors, including IL-1β (Fig. 12 J) and ZO-1 (Fig. 12 K). These results demonstrate that micromotors can effectively heal ulcerative cells.

Conclusion and challenges

Micro/nanorobots mimicking the pollen structure, characterized by a large surface area, effectively enhance bio-adhesion and have been applied in various fields, such as drug delivery, bacterial killing, tumor treatment, and tissue regeneration. Moreover, by utilizing various materials responsive to physical stimuli, the micro/nanorobots can execute specific actions triggered by external stimuli, allowing for precise control under various environmental conditions and facilitating the targeted delivery of drugs or cells. These micro/nanorobots surpass the constraints associated with conventional treatments and represent an expedited therapeutic approach. However, various challenges remain for micro/nanorobots. Numerous scientists are exploring different approaches for using micro/nanorobots in clinical settings; however, despite these ongoing efforts, functional micro/nanorobots designed for clinical applications are yet to be released. Most validation studies

involving micro/nanorobots have been conducted *in vitro*. Several limitations must be addressed in order to use micro/nanorobots *in vivo*.

Micro/nanorobot tracking monitoring

Monitoring technologies are essential for localizing and tracking micro/nanorobots in living organisms. However, this is challenging, and traditional imaging methods have limitations. Pouponneau et al. monitored the magnetic microcarriers used for tumor treatment as they reached deep tissues using an MRI system [194]. The therapeutic magnetic microcarriers developed in this study demonstrated that steering through arteries could also be achieved using an MRI system. However, clinical MRI scanners can only function through STEER millimeter-scale carriers [195,196], and delays between image processing and actuation can lead to unstable navigation control. Additionally, immediate intervention is impossible in emergencies, such as microrobot failures. Therefore, real-time observations within the body are necessary to precisely target the stability of microrobots. However, owing to the small size of microrobots and the low detection resolution of imaging devices, real-time imaging of microrobots within the body remains challenging, and additional research is required.

Biocompatibility and biodegradability

Clinical micro/nanorobots should be constructed from materials that are recognized safe for use in medical settings, specifically those that are biocompatible and biodegradable, according to standards set by regulatory bodies, such as the U.S. Food & Drug Administration. This ensures that micro/nanorobots can break down swiftly within living organisms without producing harmful byproducts or residual toxins. If micro/nanorobots are not excreted from the body or metabolized internally, robotic components can accumulate in organs and cause chronic inflammation[197]. Wang et al. reported microswimmers based on GelMA hydrogels and biodegradable proteins [198]. The helical microswimmer fabricated with GelMA underwent partial degradation due to protease secretion from the cells during the week-long cell culture. Consequently, its rigid cuboidal structure softened and eventually biodegraded. Terzopoulou et al. developed a composite magnetic metal-organic framework (MOF)-bot utilizing GelMA and a magnetic MOF designed to biodegrade within the human body.[199]. MOF composites and microrobots made with GelMA-based frameworks were fully degraded by proteolytic enzymes, such as collagenase and protease, which are secreted by various mammalian cell lines. Furthermore, the magnetic component of the MOF-bot exhibited pH-responsiveness, enhancing its utility in drug encapsulation and controlled release. Moreover, owing to the soft magnetic properties of MOF, which enable magnetic propulsion under the influence of an external magnetic field, integrated MOF-bots can deliver drugs in cell culture settings. The fabrication of these universally biodegradable micro/nanorobots underscores the importance of next-generation biomaterial-based micro/-nanorobots. This approach is essential for producing medical micro/nanorobots suitable for cell manipulation or internal bodily insertion.

Overcoming biological barriers

Vascular system

Micro/nanorobots can navigate deep within the body through vascular networks. However, given that the body's smallest capillaries measure only a few micrometers across the [200], the dimensions of these synthetic micro/nanodevices must be smaller than the internal diameters of the vessels they traverse. Larger micro/nanorobots pose a risk of obstructing the cerebral or pulmonary arteries, potentially leading to stroke or pulmonary embolism. Moreover, the dynamic viscoelastic properties of blood[201], which are influenced by vessel width, blood velocity, and hematocrit levels, present challenges for micro/nanorobot movement within the bloodstream. Tianlong et al. developed a microrobot covered with a membrane made of red blood cells featuring a claw-like structure derived from pollen particles, which enhanced its ability to stick to blood vessel walls[202]. Despite the significant intravascular flow, the microrobot remained securely connected to the blood vessel at a flow rate (FR) of 2.1 cm/s owing to its claw design. Furthermore, magnetically driven rotation in the XY plane of the veins makes it possible to keep the microrobot in blood vessels for an extended period, even with a relative blood flow (RF) of up to 3.2 cm/s. Additionally, the microrobot coating of red blood cell membrane helped avoid detection by the immune system and enabled longer circulation within the bloodstream. These findings demonstrate that the surface design of micro/nanorobots can be used to bypass obstacles in the bloodstream for the delivery of various types of drugs. The benefits of controlled movement and sustained autonomous operation within blood vessels hold significant potential for broadening the applications of these micro/nanorobots, presenting a compelling pathway for targeted drug delivery in various diseases.

Immune system

Medical micro/nanorobots require a meticulous evaluation of their interactions with the immune system. When a micro/nanorobot enters the body, the immune system identifies it as a foreign entity, prompting macrophages to ingest it and initiate phagocytosis to expel it from the body[203]. The duration of phagocytosis is influenced by the characteristics of the particle surface and dimensions[204]. Generally, micro/nanorobots inspired by pollen exhibit complex shapes that diverge from conventional simple forms, such as spheres. Therefore, to employ pollen-inspired micro/nanorobots in clinical settings, it is crucial to understand how immune responses interact with various particle types. Stealth microrobots are designed with surface modifications to prevent phagocytosis by interfering with immune cell recognition[203]. These micro/nanorobots with macrophage immunomodulatory capabilities not only open the door to clinical micro/nanorobots by overcoming biological barriers, but also indicate that they may be highly promising for fully non-immunogenic micro/-nanorobots in the future.

Blood brain barrier (BBB)

The BBB is one of the most difficult physiological barriers to overcome. It separates the brain from the rest of the body, acts as a selective physiological filter, and controls the movement of substances between the bloodstream and brain tissue. Therefore, drugs with molecular weights exceeding 500 Da struggle to penetrate the brain, leading to a reduced drug delivery efficiency [205]. Micro/nanorobots address the challenge of drug delivery across the BBB by leveraging their small size and specialized mobility. Recently, micro/nanorobots have been investigated for the treatment of brain tumors, demonstrating enhanced targeting accuracy at tumor sites[206]. Intracranial cross-targeted drug delivery nanorobots have also been reported for therapeutic drug delivery to brain [207]. The nanorobot entered the intracranial cavity in a non-invasive manner without any leakage through the pathway created by the OMMAYA cannula and successfully reached the target area. Moreover, unwanted drug release was reduced and the blood-brain barrier was successfully bypassed. They proved the biocompatibility of nanorobots and found that intracerebral treatment with these robots caused minimal damage to the brain tissue and other major organs, with no evidence of inflammation. This indicates that micro/nanorobots could be useful in the future for delivering active drugs across the BBB and potentially treating brain diseases.

The bulk of the micro/nanorobots designed to address the issues discussed earlier did not resemble pollen particles. However, we propose that by presenting and refining existing micro/nanorobots, it is possible to create micro/nanorobots modeled after pollen particles. We anticipate that addressing the various challenges faced by pollen-inspired micro/nanorobots for practical human body applications will foster

enhanced interdisciplinary collaborations, particularly in areas, such as skin and bone regeneration. Consequently, this is expected to pave the way for the advancement of cutting-edge therapies and present auspicious opportunities for the future of humankind.

Future directions

Next, studies on stimuli-actuated P-M/N bots should concentrate on precise manufacture and functionalization, broad characterization, and accurate stimuli-responsiveness measurements to advance therapeutic approaches. As the existing methods of fabrication mainly include chemical synthesis approaches, which often result in heterogeneous nanobot synthesis, the future P-M/N bots can be fabricated through advanced 3D printing technology.

3D printing has contributed significantly to various biomedical sectors, from microfluidics to laboratory/organ-on-a-chip technology [208–211]. 3D printing is more precise than traditional manufacturing methods, promises high degrees of reproducibility, automation enables tailoring, short turnaround intervals between design updates, and ensures a relatively low-cost process [212]. P-M/N bot fabrication through 3D printing technology can be achieved through any of the existing 3D printing types, including material extrusion, additive manufacturing, inkjet printing, binder jetting, two-photon polymerization, and laser freeform construction [213,214].

Even though we have yet to fabricate P-M/N bots, promising innovation is seen in pollen particles and 3D printing combined technology, inspiring us to fabricate P-M/N bots through advanced 3D printing techniques. For instance, multi-material structures with pH-responsive interiors and pollen-inspired spikes were created using photonic 3D laser printing. Natural, non-allergenic pollen particles and digital printing technology were used to build moisture-responsive bilayer structures with sophisticated deformability and functional programmability. Commercial digital printers print predesigned patterns on pollen sheets to create shape-morphing 3D combinations. The simple, eco-friendly conversion of pollen particles to paper using industrial processing machinery shows that intelligent green products with programmable and reversible mechanical properties for electronic and biomedical applications are possible [215].

In addition, biological advancements might be enhanced by the creation of hydrogel-encapsulated P-M/N bots, which now contain P-M/N particles without any actuation mechanisms. Thus, although the P-M/N structure incorporated 3D printed hydrogels have shown favorable biomedical uses, the fabrication of hydrogel-incorporated nanobots is necessary to enable further applications in the future of P-M/N bots.

It will be crucial to address difficulties like scalability, maintaining consistent production, and attaining precise control in complicated biological contexts. Methods for tackling these difficulties involve utilizing sophisticated chemical functionalization methods to improve biocompatibility and targeting abilities, incorporating various stimuli-responsive components for intelligent delivery systems, and promoting interdisciplinary collaboration among material scientists, biologists, and clinicians. Addressing these challenges will enable future studies to facilitate the use of pollen-inspired micro/nanorobots in clinical settings, leading to improved patient outcomes and progress in targeted medicinal administration. Furthermore, comprehensive *in vivo* investigations or organ-on-chip platforms are necessary to evaluate the compatibility with living organisms and potential long-term harm, including addressing concerns about immune system reactions.

Author statement

All authors (below) certify that they have taken part in the revised version of the manuscript titled “Stimuli-triggered Pollen-inspired Micro/Nanorobots for Advanced Therapeutics”. All authors take responsibility for the content. Youjin Seol, Keya Ganguly, Hojin Kim, Aayushi Randhawa, Tejal V. Patil, Sayan Deb Dutta, Rumi Acharya, Ki-Taek Lim.

CRediT authorship contribution statement

Aayushi Randhawa: Resources. **Tejal V Patil:** Resources. **Sayan Deb Dutta:** Resources. **Rumi Acharya:** Resources. **Seol youjin:** Writing – review & editing, Writing – original draft, Visualization, Investigation, Conceptualization. **Keya Ganguly:** Writing – review & editing, Writing – original draft. **Hojin Kim:** Resources. **Ki-Taek Lim:** Funding acquisition, Conceptualization.

Declaration of Competing Interest

The authors declare the following financial interests/personal relationships which may be considered as potential competing interests: Ki-Taek Lim reports financial support was provided by Government of the Republic of Korea. Ki-Taek Lim reports a relationship with Government of the Republic of Korea that includes: funding grants. If there are other authors, they declare that they have no known competing financial interests or personal relationships that could have appeared to influence the work reported in this paper.

Data availability

No data was used for the research described in the article.

Acknowledgments

Y.S. and K.G. contributed equally to this work. This study was supported by the Basic Science Research Program through the National Research Foundation of Korea funded by the Ministry of Education (NRF-2018R1A16A1A03025582, NRF-2022R1I1A3063302). This research was supported by the Ministry of Science and ICT, Korea, under the Innovative Human Resource Development for Local Intellectualization support program (IITP-2023-RS-2023-00260267*) supervised by the Institute for Information and Communications Technology Planning & Evaluation.

References

[1] P. Pacher, P. Mukhopadhyay, R. Mohanraj, G. Godlewski, S. Bátkai, G. Kunos, Hypertension 52 (2008) 601–607.
[2] T. Hackert, M.W. Büchler, Dig. Dis. 31 (2013) 51–56.
[3] A.J. Paredes, I.K. Ramöller, P.E. McKenna, M.T. Abbate, F. Volpe-Zanutto, L. K. Vora, M. Kilbourne-Brook, C. Jarrahian, K. Moffatt, C. Zhang, Adv. Drug Deliv. Rev. 173 (2021) 331–348.
[4] S.H. Kim, D.Y. Park, B.-H. Min, Tissue Eng. Regen. Med. 9 (2012) 240–248.
[5] M.W. Tibbitt, J.E. Dahlman, R. Langer, J. Am. Chem. Soc. 138 (2016) 704–717.
[6] S. Dostalova, H. Polanska, M. Svobodova, J. Balvan, O. Krystofova, Y. Haddad, S. Krizkova, M. Masarik, T. Eckschlager, M. Stiborova, Sci. Rep. 8 (2018) 8867.
[7] M. Filippi, F. Garello, O. Yasa, J. Kasamkattil, A. Scherberich, R.K. Katzschmann, Small 18 (2022) 2104079.
[8] A. Aziz, S. Pane, V. Iacovacci, N. Koukourakis, Jr Czarske, A. Menciassi, M. Medina-Sánchez, O.G. Schmidt, ACS nano 14 (2020) 10865–10893.
[9] S. Fusco, M.S. Sakar, S. Kennedy, C. Peters, R. Bottani, F. Starsich, A. Mao, G. A. Sotiriou, S. Pané, S.E. Pratsinis, Adv. Mater. 26 (2014) 952–957.
[10] W. Hu, G.Z. Lum, M. Mastrangeli, M. Sitti, Nature 554 (2018) 81–85.
[11] B.J. Nelson, I.K. Kaliakatsos, J.J. Abbott, Annu. Rev. Biomed. Eng. 12 (2010) 55–85.
[12] D.-H. Kim, P.K. Wong, J. Park, A. Levchenko, Y. Sun, Annu. Rev. Biomed. Eng. 11 (2009) 203–233.
[13] M. Sitti, H. Ceylan, W. Hu, J. Giltinan, M. Turan, S. Yim, E. Diller, Proc. IEEE 103 (2015) 205–224.
[14] J. Li, X. Li, T. Luo, R. Wang, C. Liu, S. Chen, D. Li, J. Yue, S.-h Cheng, D. Sun, Sci. Robot. 3 (2018) eaat8829.
[15] B. Wang, K. Kostarelos, B.J. Nelson, L. Zhang, Adv. Mater. 33 (2021) 2002047.
[16] M. Luo, Y. Feng, T. Wang, J. Guan, Adv. Funct. Mater. 28 (2018) 1706100.
[17] F. Araujo, C. Martins, C. Azevedo, B. Sarmento, Adv. Drug Deliv. Rev. 124 (2018) 98–106.
[18] B. Bhushan, Langmuir 28 (2012) 1698–1714.
[19] S. Ito, S.N. Gorb, ACS Appl. Mater. Interfaces 11 (2019) 24691–24698.
[20] J.M. Tylianakis, Science 339 (2013) 1532–1533.
[21] J.H. Park, J. Seo, J.A. Jackman, N.-J. Cho, Sci. Rep. 6 (2016) 28017.
[22] A.F. Edlund, R. Swanson, D. Preuss, Plant Cell 16 (2004) S84–S97.

[23] S. Barrier, University of Hull Hull, UK2008.
[24] K. Anselme, L. Ploux, A. Ponche, J. Adhes. Sci. Technol. 24 (2010) 831–852.
[25] H. Lin, I. Gomez, J.C. Meredith, Langmuir 29 (2013) 3012–3023.
[26] H. Lin, L. Lizarraga, L.A. Bottomley, J.C. Meredith, J. Colloid Interface Sci. 442 (2015) 133–139.
[27] Z. Dang, J. Sun, J. Fan, J. Li, X. Li, T. Chen, Mater. Sci. Eng.: C. 124 (2021) 112071.
[28] J. Jia, N. Metzkow, S.-M. Park, Y.L. Wu, A.D. Sample, B. Diloknawarit, I. Jung, T. W. Odom, Nano Lett. 23 (2023) 11260–11265.
[29] H. Song, Y. Ahmad Nor, M. Yu, Y. Yang, J. Zhang, H. Zhang, C. Xu, N. Mitter, C. Yu, J. Am. Chem. Soc. 138 (2016) 6455–6462.
[30] R. Fan, C. Chen, H. Hou, D. Chuan, M. Mu, Z. Liu, R. Liang, G. Guo, J. Xu, Adv. Funct. Mater. 31 (2021) 2009733.
[31] B. Garcia-Pinel, A. Ortega-Rodríguez, C. Porras-Alcalá, L. Cabeza, R. Contreras-Cáceres, R. Ortiz, A. Díaz, A. Moscoso, F. Sarabia, J. Prados, Artif. Cells, Nanomed., Biotechnol. 48 (2020) 1022–1035.
[32] J. Wang, Z. Xiong, J. Tang, Adv. Intell. Syst. 3 (2021) 2000170.
[33] P. Harder, N. İyisan, C. Wang, F. Kohler, I. Neb, H. Lahm, M. Dreßen, M. Krane, H. Dietz, B. Özkale, Adv. Healthc. Mater. (2023) 2300904.
[34] Z. Wang, Z. Xu, B. Zhu, Y. Zhang, J. Lin, Y. Wu, D. Wu, Nanotechnology 33 (2022) 152001.
[35] M. Li, J. Wu, D. Lin, J. Yang, N. Jiao, Y. Wang, L. Liu, Acta Biomater. 154 (2022) 443–453.
[36] Q. Yang, S. Tang, D. Lu, Y. Li, F. Wan, J. Li, Q. Chen, Z. Cong, X. Zhang, S. Wu, ACS Appl. Bio Mater. 5 (2022) 4425–4434.
[37] L. Cai, X. Cao, C. Zhao, Z. Luo, Y. Zhao, ACS Nano 17 (2023) 19993–20001.
[38] J. Jiang, Z. Yang, A. Ferreira, L. Zhang, Adv. Intell. Syst. 4 (2022) 2100279.
[39] Y. Zhou, M. Ye, C. Hu, H. Qian, B.J. Nelson, X. Wang, ACS Nano 17 (2023) 15254–15276.
[40] T. He, Y. Yang, X.-B. Chen, Micromachines 14 (2023) 2253.
[41] L. Hu, T. Shu, Y. Wan, C. Fang, F. Gao, M.J. Serpe, Mol. Syst. Des. Eng. 6 (2021) 108–121.
[42] D. Wang, X. Han, B. Dong, F. Shi, Appl. Mater. Today 25 (2021) 101250.
[43] A. Marjani, R. Soltani, M. Pishnamazi, M. Rezakazemi, S. Shirazian, Microporous Mesoporous Mater. 310 (2021) 110531.
[44] L. Cai, C. Zhao, X. Cao, M. Lu, N. Li, Y. Luo, Y. Wang, Y. Zhao, Bioact. Mater. 32 (2024) 28–36.
[45] L. Song, S. Zhang, Q. Wang, W. Chen, B. Liu, Y.-D. Zhao, Chem. Eng. J. 435 (2022) 135067.
[46] Y.-W. Lee, J.-K. Kim, U. Bozuyuk, N.O. Dogan, M.T.A. Khan, A. Shiva, A.-M. Wild, M. Sitti, Adv. Mater. 35 (2023) 2209812.
[47] D. Liu, T. Zhang, Y. Guo, Y. Liao, Z. Wu, H. Jiang, Y. Lu, ACS Appl. Bio Mater. 5 (2022) 5933–5942.
[48] C.C. Mayorga-Martinez, M. Fojtů, J. Vyskočil, N.-J. Cho, M. Pumera, Adv. Funct. Mater. 32 (2022) 2207272.
[49] B. Cai, M. Zhao, Y. Ma, Z. Ye, J. Huang, ACS Appl. Mater. Interfaces 7 (2015) 1327–1333.
[50] A. Diego-Taboada, S.T. Beckett, S.L. Atkin, G. Mackenzie, Pharmaceutics 6 (2014) 80–96.
[51] E. Pacini, G.G. Franchi, Bot. J. Linn. Soc. 193 (2020) 141–164.
[52] G. Bohne, E. Richter, H. Woehlecke, R. Ehwald, Ann. Bot. 92 (2003) 289–297.
[53] R.C. Mundargi, M.G. Potroz, J.H. Park, J. Seo, E.-L. Tan, J.H. Lee, N.-J. Cho, Sci. Rep. 6 (2016) 19960.
[54] T. Ariizumi, K. Toriyama, Annu. Rev. Plant Biol. 62 (2011) 437–460.
[55] E. Pacini, M. Hesse, Flora-Morphol., Distrib. Funct. Ecol. Plants 200 (2005) 399–415.
[56] H. Lin, L. Lizarraga, L.A. Bottomley, J. Carson Meredith, J. Colloid Interface Sci. 442 (2015) 133–139.
[57] S. Ourani-Pourdashti, A. Azadi, J. Control. Release 340 (2021) 308–317.
[58] X. Sun, M. Li, Y. Yang, H. Jia, W. Liu, Biomater. Sci. 6 (2018) 3300–3308.
[59] S. Wang, M. Chen, L. Wu, ACS Appl. Mater. Interfaces 8 (2016) 33316–33325.
[60] J.M. Ageitos, S. Robla, L. Valverde-Fraga, M. Garcia-Fuentes, N. Csaba, Polymers 13 (2021) 2094.
[61] G. D'Amato, H.J. Chong-Neto, O.P. Monge Ortega, C. Vitale, I. Ansotegui, N. Rosario, T. Haahtela, C. Galan, R. Pawankar, M. Murrieta-Aguttes, Allergy 75 (2020) 2219–2228.
[62] A. Kurganskiy, S. Creer, N. De Vere, G.W. Griffith, N.J. Osborne, B.W. Wheeler, R. N. McInnes, Y. Clewlow, A. Barber, G.L. Brennan, Sci. Adv. 7 (2021) eabd7658.
[63] S.V. Lale, H.S. Gill, Int. J. Pharm. 552 (2018) 352–359.
[64] T. Maric, M.Z.M. Nasir, N.F. Rosli, M. Budanović, R.D. Webster, N.-J. Cho, M. Pumera, Adv. Funct. Mater. 30 (2020) 2000112.
[65] S.V. Lale, H.S. Gill, Int. J. Pharm. 552 (2018) 352–359.
[66] J. Huang, X. Han, D. Wang, D. Liu, T. You, ACS Appl. Mater. Interfaces 5 (2013) 9148–9154.
[67] X. Cui, P. Xiao, J. Wang, M. Zhou, W. Guo, Y. Yang, Y. He, Z. Wang, Y. Yang, Y. Zhang, Angew. Chem. Int. Ed. 56 (2017) 4488–4493.
[68] G. Zhang, S. Sun, M.N. Banis, R. Li, M. Cai, X. Sun, Cryst. Growth Des. 11 (2011) 2493–2499.
[69] P. Zhang, L. Chen, T. Xu, H. Liu, X. Liu, J. Meng, G. Yang, L. Jiang, S. Wang, Adv. Mater. 25 (2013) 3566–3570.
[70] T.K. Sau, A.L. Rogach, F. Jäckel, T.A. Klar, J. Feldmann, Adv. Mater. 22 (2010) 1805–1825.
[71] A.R. Tao, S. Habas, P. Yang, Small 4 (2008) 310–325.
[72] K.L. Kelly, E. Coronado, L.L. Zhao, G.C. Schatz, ACS Publ. (2003) 668–677.
[73] E.E. Coughlin, J. Hu, A. Lee, T.W. Odom, J. Am. Chem. Soc. 143 (2021) 3671–3676.
[74] K. Dardir, H. Wang, B.E. Martin, M. Atzampou, C.B. Brooke, L. Fabris, J. Phys. Chem. C. 124 (2020) 3211–3217.
[75] Y. Jiang, X.-J. Wu, Q. Li, J. Li, D. Xu, Nanotechnology 22 (2011) 385601.
[76] E. Hao, R.C. Bailey, G.C. Schatz, J.T. Hupp, S. Li, Nano Lett. 4 (2004) 327–330.
[77] T.K. Sau, C.J. Murphy, J. Am. Chem. Soc. 126 (2004) 8648–8649.
[78] W. Kim, W. Lee, H. Park, J. Park, W. Kim, B. Kang, E. Choi, C.-S. Kim, J.-O. Park, G. Lee, ACS Sustain. Chem. Eng. 10 (2022) 3180–3190.
[79] Z.L. Wang, J. Song, Science 312 (2006) 242–246.
[80] R.S. Devan, R.A. Patil, J.H. Lin, Y.R. Ma, Adv. Funct. Mater. 22 (2012) 3326–3370.
[81] J.N. Schrauben, R. Hayoun, C.N. Valdez, M. Braten, L. Fridley, J.M. Mayer, Science 336 (2012) 1298–1301.
[82] P. Sharma, J.B. Shin, B.C. Park, J.-W. Lee, S.W. Byun, N.-Y. Jang, Y.J. Kim, Y. Kim, Y.K. Kim, N.-H. Cho, Nanoscale 11 (2019) 4591–4600.
[83] P.B. Ezhuthupurakkal, S. Ariraman, S. Arumugam, N. Subramaniyan, S. K. Muthuvel, P. Kumpati, B. Rajamani, T. Chinnasamy, Nanomed. Nanotechnol., Biol. Med. 14 (2018) 415–428.
[84] H. Fukui, M. Horie, S. Endoh, H. Kato, K. Fujita, K. Nishio, L.K. Komaba, J. Maru, A. Miyauhi, A. Nakamura, Chem. Biol. Interact. 198 (2012) 29–37.
[85] S. Ostrovsky, G. Kazimirsky, A. Gedanken, C. Brodie, Nano Res. 2 (2009) 882–890.
[86] R. Wahab, N.K. Kaushik, A.K. Verma, A. Mishra, I. Hwang, Y.-B. Yang, H.-S. Shin, Y.-S. Kim, JBIC J. Biol. Inorg. Chem. 16 (2011) 431–442.
[87] T. Yanagisawa, T. Shimizu, K. Kuroda, C. Kato, Bull. Chem. Soc. Jpn. 63 (1990) 988–992.
[88] C. Kresge, M.E. Leonowicz, W.J. Roth, J. Vartuli, J. Beck, a, Nature 359 (1992) 710–712.
[89] M. Yu, Y. Niu, J. Zhang, H. Zhang, Y. Yang, E. Taran, S. Jambhrunkar, W. Gu, P. Thorn, C. Yu, Nano Res. 9 (2016) 291–305.
[90] N. Zhao, X. Lin, Q. Zhang, Z. Ji, F.J. Xu, Small 11 (2015) 6467–6479.
[91] X. Lin, N. Zhao, P. Yan, H. Hu, F.-J. Xu, Acta Biomater. 11 (2015) 381–392.
[92] Y. Chen, Q. Meng, M. Wu, S. Wang, P. Xu, H. Chen, Y. Li, L. Zhang, L. Wang, J. Shi, J. Am. Chem. Soc. 136 (2014) 16326–16334.
[93] X. Du, B. Shi, Y. Tang, S. Dai, S.Z. Qiao, Biomaterials 35 (2014) 5580–5590.
[94] Y. Wan, Zhao, Chem. Rev. 107 (2007) 2821–2860.
[95] F. Hoffmann, M. Cornelius, J. Morell, M. Fröba, Angew. Chem. Int. Ed. 45 (2006) 3216–3251.
[96] I.I. Slowing, J.L. Vivero-Escoto, B.G. Trewyn, V.S.-Y. Lin, J. Mater. Chem. 20 (2010) 7924–7937.
[97] R. Jin, J. Wang, M. Gao, X. Zhang, Talanta 231 (2021) 122402.
[98] R.C. Mundargi, M.G. Potroz, S. Park, H. Shirahama, J.H. Lee, J. Seo, N.-J. Cho, Small 12 (2016) 1167–1173.
[99] S.A. Hamad, A.F.K. Dyab, S.D. Stoyanov, V.N. Paunov, J. Mater. Chem. 21 (2011) 18018–18023.
[100] T. Fan, J.H. Park, Q.A. Pham, E.-L. Tan, R.C. Mundargi, M.G. Potroz, H. Jung, N.-J. Cho, Sci. Rep. 8 (2018) 6565.
[101] T.-F. Fan, S. Park, Q. Shi, X. Zhang, Q. Liu, Y. Song, H. Chin, M.S.B. Ibrahim, N. Mokrzecka, Y. Yang, H. Li, J. Song, S. Suresh, N.-J. Cho, Nat. Commun. 11 (2020) 1449.
[102] S.U. Atwe, Y. Ma, H.S. Gill, J. Control. Release 194 (2014) 45–52.
[103] H. Hamrouni, I. Jaouali, M. Nsib, E. Fazio, F. Neri, A. Bonavita, S.G. Leonardi, G. Neri, J. Mater. Sci.: Mater. Electron. 29 (2018) 11096–11103.
[104] R.D. Ávila-Avilés, N. Torres-Gómez, M.A. Camacho-López, A.R. Vilchis-Nestor, Sci. Rep. 10 (2020) 16633.
[105] P.-M. Chen, W.-Y. Pan, P.-K. Luo, H.N. Phung, Y.-M. Liu, M.-C. Chiang, W.-A. Chang, T.-L. Tien, C.-Y. Huang, W.-W. Wu, W.-T. Chia, H.-W. Sung, ACS Nano 15 (2021) 7596–7607.
[106] L. Shi, J. Cao, C. Yang, X. Wang, K. Shi, L. Shang, J. Colloid Interface Sci. 615 (2022) 408–416.
[107] J. Li, F. Ji, D.H. Ng, J. Liu, X. Bing, P. Wang, Chem. Eng. J. 369 (2019) 611–620.
[108] B. Jurado-Sánchez, M. Pacheco, J. Rojo, A. Escarpa, Angew. Chem. Int. Ed. 56 (2017) 6957–6961.
[109] Y. Dong, L. Wang, K. Yuan, F. Ji, J. Gao, Z. Zhang, X. Du, Y. Tian, Q. Wang, L. Zhang, ACS Nano 15 (2021) 5056–5067.
[110] Q. Wang, L. Yang, J. Yu, L. Zhang, 2017 IEEE International Conference on Robotics and Biomimetics (ROBIO), IEEE2017, pp. 1442-1447.
[111] A. Bonilla-Brunner, I.L. García, B. Jang, M.A. Patino, V. Alimchandani, B. J. Nelson, S. Pané, S. Contera, Appl. Mater. Today 18 (2020) 100511.
[112] L. Xie, X. Pang, X. Yan, Q. Dai, H. Lin, J. Ye, Y. Cheng, Q. Zhao, X. Ma, X. Zhang, ACS nano 14 (2020) 2880–2893.
[113] A.I. Bunea, D. Martella, S. Nocentini, C. Parmeggiani, R. Taboryski, D.S. Wiersma, Adv. Intell. Syst. 3 (2021) 2000256.
[114] W. Jiang, D. Niu, H. Liu, C. Wang, T. Zhao, L. Yin, Y. Shi, B. Chen, Y. Ding, B. Lu, Adv. Funct. Mater. 24 (2014) 7598–7604.
[115] G. Go, H. Choi, C. Lee, S.Y. Ko, J.-O. Park, S. Park, 2016 6th IEEE International Conference on Biomedical Robotics and Biomechatronics (BioRob), IEEE2016, pp. 1186-1191.
[116] V. Iacovacci, A. Blanc, H. Huang, L. Ricotti, R. Schibli, A. Menciassi, M. Behe, S. Pané, B.J. Nelson, Small 15 (2019) 1900709.
[117] S.N. Tabatabaei, J. Lapointe, S. Martel, Adv. Robot. 25 (2011) 1049–1067.
[118] F. Mou, C. Chen, Q. Zhong, Y. Yin, H. Ma, J. Guan, ACS Appl. Mater. Interfaces 6 (2014) 9897–9903.
[119] D.-i Kim, H. Lee, S.-h Kwon, H. Choi, S. Park, Sens. Actuators B: Chem. 289 (2019) 65–77.

[120] J. Li, P. Angsantikul, W. Liu, B. Esteban-Fernández de Ávila, S. Thamphiwatana, M. Xu, E. Sandraz, X. Wang, J. Delezuk, W. Gao, Angew. Chem. Int. Ed. 56 (2017) 2156–2161.
[121] D. Jin, Q. Chen, T.-Y. Huang, J. Huang, L. Zhang, H. Duan, Mater. Today 32 (2020) 19–25.
[122] M. Dong, X. Wang, X.Z. Chen, F. Mushtaq, S. Deng, C. Zhu, H. Torlakcik, A. Terzopoulou, X.H. Qin, X. Xiao, Adv. Funct. Mater. 30 (2020) 1910323.
[123] C.C. Mayorga-Martinez, M. Fojtů, J. Vyskočil, N.J. Cho, M. Pumera, Adv. Funct. Mater. 32 (2022) 2207272.
[124] M. Sitti, D.S. Wiersma, Adv. Mater. 32 (2020) 1906766.
[125] L. Xu, F. Mou, H. Gong, M. Luo, J. Guan, Chem. Soc. Rev. 46 (2017) 6905–6926.
[126] J. Zhang, J. Guo, F. Mou, J. Guan, Micromachines 9 (2018) 88.
[127] U. Bozuyuk, O. Yasa, I.C. Yasa, H. Ceylan, S. Kizilel, M. Sitti, ACS Nano 12 (2018) 9617–9625.
[128] X. Song, Z. Chen, X. Zhang, J. Xiong, T. Jiang, Z. Wang, X. Geng, U.K. Cheang, Sci. Rep. 11 (2021) 7907.
[129] L. Song, J. Cai, S. Zhang, B. Liu, Y.-D. Zhao, W. Chen, Sens. Actuators B: Chem. 358 (2022) 131523.
[130] Y. Ying, A.M. Pourrahimi, C.L. Manzanares-Palenzuela, F. Novotny, Z. Sofer, M. Pumera, Small 16 (2020) 1902944.
[131] A.M. Pourrahimi, K. Villa, C.L. Manzanares Palenzuela, Y. Ying, Z. Sofer, M. Pumera, Adv. Funct. Mater. 29 (2019) 1808678.
[132] V. Sridhar, F. Podjaski, J. Kröger, A. Jiménez-Solano, B.-W. Park, B.V. Lotsch, M. Sitti, Proc. Natl. Acad. Sci. 117 (2020) 24748–24756.
[133] K. Cai, J. Yu, J. Shi, Q.H. Qin, J. Phys. Chem. C. 121 (2017) 16985–16995.
[134] E. Gultepe, J.S. Randhawa, S. Kadam, S. Yamanaka, F.M. Selaru, E.J. Shin, A. N. Kalloo, D.H. Gracias, Adv. Mater. 25 (2013) 514–519.
[135] H.-W. Huang, M.S. Sakar, A.J. Petruska, S. Pané, B.J. Nelson, Nat. Commun. 7 (2016) 12263.
[136] C. Fiedler, C. Ulbricht, T. Truglas, D. Wielend, M. Bednorz, H. Groiss, O. Brüggemann, I. Teasdale, Y. Salinas, Chem. A Eur. J. 27 (2021) 3262–3267.
[137] H. Lee, H. Choi, M. Lee, S. Park, Biomed. Micro 20 (2018) 1–9.
[138] Y.W. Lee, J.K. Kim, U. Bozuyuk, N.O. Dogan, M.T.A. Khan, A. Shiva, A.M. Wild, M. Sitti, Adv. Mater. 35 (2023) 2209812.
[139] N.S. Satarkar, J.Z. Hilt, J. Control. Release 130 (2008) 246–251.
[140] E. Proksch, J. Dermatol. 45 (2018) 1044–1052.
[141] F. Iemma, U.G. Spizzirri, F. Puoci, R. Muzzalupo, S. Trombino, R. Cassano, S. Leta, N. Picci, Int. J. Pharm. 312 (2006) 151–157.
[142] C. Alvarez-Lorenzo, A. Concheiro, From drug dosage forms to intelligent drug-delivery systems: a change of paradigm, Smart materials for drug delivery, R. Soc. Chem. (2013) 1–32.
[143] G.K. Such, Y. Yan, A.P. Johnston, S.T. Gunawan, F. Caruso, Adv. Mater. 27 (2015) 2278–2297.
[144] G. Fuhrmann, A. Serio, M. Mazo, R. Nair, M.M. Stevens, J. Control. Release 205 (2015) 35–44.
[145] S. Shang, X. Li, H. Wang, Y. Zhou, K. Pang, P. Li, X. Liu, M. Zhang, W. Li, Q. Li, Bioact. Mater. 37 (2024) 206–221.
[146] M. Sun, X. Fan, X. Meng, J. Song, W. Chen, L. Sun, H. Xie, Nanoscale 11 (2019) 18382–18392.
[147] B. Hawthorne, J.K. Simmons, B. Stuart, R. Tung, D.S. Zamierowski, A.J. Mellott, J. Biomed. Mater. Res. Part B: Appl. Biomater. 109 (2021) 1967–1985.
[148] D.T. Debela, S.G. Muzazu, K.D. Heraro, M.T. Ndalama, B.W. Mesele, D.C. Haile, S. K. Kitui, T. Manyazewal, SAGE Open Med. 9 (2021), 20503121211034366.
[149] F. Shahraki, M.H. Tabrizi, M.N. Moghaddam, S. Hajebi, IET Nanobiotechnol. 13 (2019) 471–476.
[150] M.F. Salas-Orozco, A.C. Lorenzo-Leal, I. de Alba Montero, N.P. Marín, M.A. C. Santana, H. Bach, Nanomed. Nanotechnol. Biol. Med. 55 (2024) 102715.
[151] P. Horcajada, T. Chalati, C. Serre, B. Gillet, C. Sebrie, T. Baati, J.F. Eubank, D. Heurtaux, P. Clayette, C. Kreuz, Nat. Mater. 9 (2010) 172–178.
[152] K.-J. Chen, H.-F. Liang, H.-L. Chen, Y. Wang, P.-Y. Cheng, H.-L. Liu, Y. Xia, H.-W. Sung, ACS Nano 7 (2013) 438–446.
[153] Y. Liu, L. Feng, T. Liu, L. Zhang, Y. Yao, D. Yu, L. Wang, N. Zhang, Nanoscale 6 (2014) 3231–3242.
[154] R. Gui, A. Wan, X. Liu, H. Jin, Chem. Commun. 50 (2014) 1546–1548.
[155] S.-H. Hu, S.-Y. Chen, D.-M. Liu, C.-S. Hsiao, Adv. Mater. 20 (2008), 2690-+.
[156] S.J. Archibald, S.L. Atkin, W. Bras, A. Diego-Taboada, G. Mackenzie, J.F. W. Mosselmans, S. Nikitenko, P.D. Quinn, M.F. Thomas, N.A. Young, J. Mater. Chem. B 2 (2014) 945–959.
[157] H. Ma, P. Zhang, J. Wang, X. Xu, H. Zhang, Z. Zhang, Y. Zhang, Y. Ning, J. Microencapsul. 31 (2014) 667–673.
[158] S. Barrier, A.S. Rigby, A. Diego-Taboada, M.J. Thomasson, G. Mackenzie, S. L. Atkin, LWT - Food Sci. Technol. 43 (2010) 73–76.
[159] A. Diego-Taboada, P. Cousson, E. Raynaud, Y. Huang, M. Lorch, B.P. Binks, Y. Queneau, A.N. Boa, S.L. Atkin, S.T. Beckett, G. Mackenzie, J. Mater. Chem. 22 (2012) 9767–9773.
[160] A. Wakil, G. Mackenzie, A. Diego-Taboada, J.G. Bell, S.L. Atkin, Lipids 45 (2010) 645–649.
[161] M. Lorch, M.J. Thomasson, A. Diego-Taboada, S. Barrier, S.L. Atkin, G. Mackenzie, S.J. Archibald, Chem. Commun. (2009) 6442–6444.
[162] S. Iravani, R.S. Varma, Nano-Micro Lett. 13 (2021) 128.
[163] H. Rosen, T. Abribat, Nat. Rev. Drug Discov. 4 (2005) 381–385.
[164] J.A. Finbloom, C. Huynh, X. Huang, T.A. Desai, Nat. Rev. Bioeng. 1 (2023) 139–152.
[165] M. KUROKI, N. SHIRASU, Anticancer Res. 34 (2014) 4481–4488.
[166] M. Magro, A. Venerando, A. Macone, G. Canettieri, E. Agostinelli, F. Vianello, Biomolecules 10 (2020) 735.
[167] 2020, Nat. Cancer 11–2.
[168] W. Gao, J. Wang, Nanoscale 6 (2014) 10486–10494.
[169] S. Mallick, R. Abouomar, D. Rivas, M. Sokolich, F.C. Kirmizitas, A. Dutta, S. Das, Adv. Healthc. Mater. 12 (2023) 2300939.
[170] H. Lee, D.-i Kim, S.-h Kwon, S. Park, ACS Appl. Mater. Interfaces 13 (2021) 19633–19647.
[171] Y. Liu, P. Bhattarai, Z. Dai, X. Chen, Chem. Soc. Rev. 48 (2019) 2053–2108.
[172] J.-J. Hu, Y.-J. Cheng, X.-Z. Zhang, Nanoscale 10 (2018) 22657–22672.
[173] R. Vankayala, K.C. Hwang, Adv. Mater. 30 (2018) 1706320.
[174] Z. Sun, H. Xie, S. Tang, X.-F. Yu, Z. Guo, J. Shao, H. Zhang, H. Huang, H. Wang, P. K. Chu, Angew. Chem. Int. Ed. 54 (2015) 11526–11530.
[175] Y. Yang, Q. Zhang, J. Zhang, A. Chen, Y. Chen, S. Li, M. Ye, X. Xuan, X. Li, H. He, J. Wu, Mater. Des. 202 (2021) 109573.
[176] W. Song, Y. Li, Y. Wang, D. Wang, D. He, W. Chen, W. Yin, W. Yang, J. Biomed. Nanotechnol. 13 (2017) 1115–1123.
[177] M. Yan, Q. Chen, T. Liu, X. Li, P. Pei, L. Zhou, S. Zhou, R. Zhang, K. Liang, J. Dong, Nat. Commun. 14 (2023) 4628.
[178] C. Xu, Y. Liu, J. Li, P. Ning, Z. Shi, W. Zhang, Z. Li, R. Zhou, Y. Tong, Y. Li, C. Lv, Y. Shen, Q. Cheng, B. He, Y. Cheng, Adv. Mater. 35 (2023) 2204996.
[179] M. Yan, Q. Chen, T. Liu, X. Li, P. Pei, L. Zhou, S. Zhou, R. Zhang, K. Liang, J. Dong, X. Wei, J. Wang, O. Terasaki, P. Chen, Z. Gu, L. Jiang, B. Kong, Nat. Commun. 14 (2023) 4628.
[180] J.M.V. Makabenta, A. Nabawy, C.-H. Li, S. Schmidt-Malan, R. Patel, V.M. Rotello, Nat. Rev. Microbiol. 19 (2021) 23–36.
[181] P. Walvekar, R. Gannimani, T. Govender, Eur. J. Pharm. Sci. 127 (2019) 121–141.
[182] Y. Wang, A. Shukla, Biomater. Sci. 10 (2022) 2831–2843.
[183] J.A. Finbloom, P. Raghavan, M. Kwon, B.N. Kharbikar, M.A. Yu, T.A. Desai, bioRxiv (2022), 2021.2011.2022.469570.
[184] D.P. Linklater, V.A. Baulin, S. Juodkazis, R.J. Crawford, P. Stoodley, E.P. Ivanova, Nat. Rev. Microbiol. 19 (2021) 8–22.
[185] M. Ganjian, K. Modaresifar, M.R.O. Ligeon, L.B. Kunkels, N. Tümer, L. Angeloni, C.W. Hagen, L.G. Otten, P.-L. Hagedoorn, I. Apachitei, L.E. Fratila-Apachitei, A. A. Zadpoor, Adv. Mater. Interfaces 6 (2019) 1900640.
[186] C.D. Bandara, S. Singh, I.O. Afara, A. Wolff, T. Tesfamichael, K. Ostrikov, A. Oloyede, ACS Appl. Mater. Interfaces 9 (2017) 6746–6760.
[187] A. Elbourne, R.J. Crawford, E.P. Ivanova, J. Colloid Interface Sci. 508 (2017) 603–616.
[188] C. Zheng, Z. Li, T. Xu, L. Chen, F. Fang, D. Wang, P. Dai, Q. Wang, X. Wu, X. Yan, Appl. Mater. Today 22 (2021) 100962.
[189] X.V. Li, I. Leonardi, G.G. Putzel, A. Semon, W.D. Fiers, T. Kusakabe, W.-Y. Lin, I. H. Gao, I. Doron, A. Gutierrez-Guerrero, M.B. DeCelie, G.M. Carriche, M. Mesko, C. Yang, J.R. Naglik, B. Hube, E.J. Scherl, I.D. Iliev, Nature 603 (2022) 672–678.
[190] Y. Cao, J. Oh, M. Xue, W.J. Huh, J. Wang, J.A. Gonzalez-Hernandez, T.A. Rice, A. L. Martin, D. Song, J.M. Crawford, Science 378 (2022) eabm3233.
[191] J.-Y. Lee, J.A. Hall, L. Kroehling, L. Wu, T. Najar, H.H. Nguyen, W.-Y. Lin, S. T. Yeung, H.M. Silva, D. Li, Cell 180 (2020) 79–91, e16.
[192] S. Zhang, R. Langer, G. Traverso, Nano Today 16 (2017) 82–96.
[193] E.L. McConnell, H.M. Fadda, A.W. Basit, Int. J. Pharm. 364 (2008) 213–226.
[194] P. Pouponneau, J.-C. Leroux, G. Soulez, L. Gaboury, S. Martel, Biomaterials 32 (2011) 3481–3486.
[195] J.-B. Mathieu, S. Martel, Biomed. Micro 9 (2007) 801–808.
[196] S. Martel, J.-B. Mathieu, O. Felfoul, A. Chanu, E. Aboussouan, S. Tamaz, P. Pouponneau, L.H. Yahia, G. Beaudoin, G. Soulez, M. Mankiewicz, Appl. Phys. Lett. 90 (2007).
[197] A. Nel, T. Xia, L. Mädler, N. Li, Science 311 (2006) 622–627.
[198] X. Wang, X.-H. Qin, C. Hu, A. Terzopoulou, X.-Z. Chen, T.-Y. Huang, K. Maniura-Weber, S. Pané, B.J. Nelson, Adv. Funct. Mater. 28 (2018) 1804107.
[199] A. Terzopoulou, X. Wang, X.-Z. Chen, M. Palacios-Corella, C. Pujante, J. Herrero-Martín, X.-H. Qin, J. Sort, A.J. deMello, B.J. Nelson, J. Puigmartí-Luis, S. Pané, Adv. Healthc. Mater. 9 (2020) 2001031.
[200] K.P. Ivanov, M.K. Kalinina, Y.I. Levkovich, Microvasc. Res. 22 (1981) 143–155.
[201] Z. Mimouni, Open J. Biophys. 6 (2016) 29–33.
[202] T. Li, S. Yu, B. Sun, Y. Li, X. Wang, Y. Pan, C. Song, Y. Ren, Z. Zhang, K.T. V. Grattan, Z. Wu, J. Zhao, Sci. Adv. 9 (2023) eadg4501.
[203] I.C. Yasa, H. Ceylan, U. Bozuyuk, A.-M. Wild, M. Sitti, Sci. Robot. 5 (2020) eaaz3867.
[204] J.A. Champion, A. Walker, S. Mitragotri, Pharm. Res. 25 (2008) 1815–1821.
[205] W.A. Banks, Nat. Rev. Drug Discov. 15 (2016) 275–292.
[206] H. Chen, T. Li, Z. Liu, S. Tang, J. Tong, Y. Tao, Z. Zhao, N. Li, C. Mao, J. Shen, M. Wan, Nat. Commun. 14 (2023) 941.
[207] J. Wu, N. Jiao, D. Lin, N. Li, T. Ma, S. Tung, W. Cheng, A. Wu, L. Liu, Adv. Mater. 36 (2024) 2306876.
[208] M. Ustun, S. Rahmani Dabbagh, I.S. Ilci, T. Bagci-Onder, S. Tasoglu, Micromachines 12 (2021) 490.
[209] A. Zargaryan, N. Farhoudi, G. Haworth, J.F. Ashby, S.H. Au, Sci. Rep. 10 (2020) 18379.
[210] V. Carvalho, I. Gonçalves, T. Lage, R.O. Rodrigues, G. Minas, S.F. Teixeira, A. S. Moita, T. Hori, H. Kaji, R.A. Lima, Sensors 21 (2021) 3304.
[211] E. Fu, L. Wentland, Lab a Chip 22 (2022) 9–25.
[212] J. Li, C. Wu, P.K. Chu, M. Gelinsky, Mater. Sci. Eng.: R: Rep. 140 (2020) 100543.
[213] S.C. Ligon, R. Liska, Jr Stampfl, M. Gurr, R. Mulhaupt, Chem. Rev. 117 (2017) 10212–10290.
[214] A. Kumar, S. Mandal, S. Barui, R. Vasireddi, U. Gbureck, M. Gelinsky, B. Basu, Mater. Sci. Eng.: R: Rep. 103 (2016) 1–39.
[215] Z. Zhao, J. Kumar, Y. Hwang, J. Deng, M.S.B. Ibrahim, C. Huang, S. Suresh, N.-J. Cho, Proc. Natl. Acad. Sci. 118 (2021) e2113715118.